



How reliable are CMIP5 models in simulating dust optical depth?

Bing Pu^{1,2} and Paul Ginoux²

¹Atmospheric and Oceanic Sciences Program, Princeton University,

Princeton, New Jersey 08544

²NOAA Geophysical Fluid Dynamics Laboratory, Princeton, New Jersey 08540

Correspondence to: Bing Pu (bpu@princeton.edu)



1 **Abstract.** Dust aerosol plays an important role in the climate system by affecting the
2 radiative and energy balances. Biases in dust modeling may result in biases in simulating
3 global energy budget and regional climate. It is thus very important to understand how
4 well dust is simulated in the Coupled Model Intercomparison Project Phase 5 (CMIP5)
5 models. Here seven CMIP5 models using interactive dust emission schemes are
6 examined against satellite derived dust optical depth (DOD) during 2004-2016.

7 It is found that multi-model mean can largely capture the global spatial pattern
8 and zonal mean of DOD over land in present-day climatology in MAM and JJA. Global
9 mean land DOD is underestimated by -25.2% in MAM to -6.4% in DJF. While seasonal
10 cycle, magnitude, and spatial pattern are generally captured by multi-model mean over
11 major dust source regions such as North Africa and the Middle East, these variables are
12 not so well represented by most of the models in South Africa and Australia. Interannual
13 variations of DOD are neither captured by most of the models nor by multi-model mean.
14 Models also do not capture the observed connections between DOD and local controlling
15 factors such as surface wind speed, bareness, and precipitation. The constraints from
16 surface bareness are largely underestimated while the influences of surface wind and
17 precipitation are overestimated.

18 Projections of DOD change in the late half of the 21st century under the
19 Representative Concentration Pathways 8.5 scenario by multi-model mean is compared
20 with those projected by a regression model. Despite the uncertainties associated with both
21 projections, results show some similarities between the two, e.g., DOD pattern over
22 North Africa in DJF and JJA, an increase of DOD in the Arabian Peninsula in all seasons,
23 and a decrease over northern China from MAM to SON.



24 1. Introduction

25 Dust is the second most abundant aerosols by mass in the atmosphere after sea
26 salt. It absorbs and scatters both shortwave and longwave radiation and thus modifies
27 local radiative budget and consequently vertical temperature profile, influencing global
28 and regional climate. For instance, studies found dust influences the strength of the West
29 African monsoon (e.g., Miller and Tegen, 1998; Miller et al., 2004; Mahowald et al.,
30 2010; Strong et al., 2015) and Indian monsoonal rainfall (e.g., Vinoj et al., 2014; Jin et
31 al., 2014, 2015, 2016; Solmon et al., 2015; Kim et al., 2016; Sharma and Miller, 2017).
32 Dust aerosols are also found to amplify droughts during the U.S. Dust Bowl and
33 Medieval Climate Anomaly (Cook et al., 2008, 2009, 2013), and affect Atlantic tropical
34 cyclones (e.g., Dunion and Velden, 2004; Wong and Dessler, 2005; Evan et al., 2006;
35 Sun et al., 2008; Strong et al., 2018). Dust particles can also serve as ice cloud nuclei and
36 influence the properties of the cloud (e.g., Levin et al., 1996; Rosenfield et al., 1997;
37 Wurzler et al., 2000; Nakajima et al., 2001; Bangert et al., 2012) and affect regional
38 radiative balance and hydrological cycle. When deposited in the oceans, iron-enriched
39 dust also provides nutrients for phytoplankton, affecting ocean productivity and therefore
40 carbon and nitrogen cycles and ocean albedo (e.g., Fung et al., 2000; Shao et al., 2011;
41 Jickells et al., 2005).

42 Globally, the estimated radiative forcing from dust aerosol is 0.10 (-0.30 to +0.10)
43 W m^{-2} , a magnitude about one fourth of the radiative forcing of sulfate aerosol or black
44 carbon from fossil fuel and biofuel (Myhre et al., 2013; their Table 8.4). Biases in dust
45 simulation may potentially affect global energy budgets and regional climate simulation.



46 Thus, it is very important to examine the capability of current state-of-the-art climate
47 models in simulating dust.

48 Only a few studies examined the Coupled Model Intercomparison Project Phase 5
49 (CMIP5) model output of dust and most of them are regional evaluations. For instance,
50 Evan et al. (2014) examined model output for Africa, but mainly focused on an area over
51 the northeastern Atlantic (10° – 20° N and 20° – 30° W) where a long-term proxy of dust
52 optical depth data over Cape Verde islands is available (Evan and Mukhopadhyay, 2010).
53 They found models underestimated dust emission and mass path and failed to capture the
54 interannual variations from 1960 to 2004, as models did not capture the negative
55 connection between dust mass path and precipitation over the Sahel.

56 Another work examined CMIP5 aerosol optical depth (AOD) is by Sanap et al.
57 (2014) for India. They compared dust distribution in the models with Earth Probe total
58 ozone monitoring system (EPTOMS)/ Ozone monitoring Instrument (OMI) aerosol index
59 (AI) from 2000 to 2005. They found most of CMIP5 models, except two HadGEM2
60 models, underestimated dust load over Indo-Gangetic Plains, and suggested the biases are
61 due to a misrepresentation of 850 hPa winds in the models. Later, Misra et al. (2016) also
62 examined CMIP5 modeled AOD for India but did not specifically focus on dust.

63 Shindell et al. (2013) examined the output of 10 models from the Atmospheric
64 Chemistry and Climate Model Intercomparison Project (ACCMIP) for one year (2000),
65 among which eight models also participated in the CMIP5. They noticed that simulated
66 dust AOD vary by more than a factor of two across models. However, this study also did
67 not focus on dust, but emphasized the radiative forcings from anthropogenic aerosols.



68 None of the above studies examined global dust simulation in CMIP5 models.
69 What's more, most studies focused on annual mean, not seasonal averages. It is very
70 possible that models perform better in some seasons than others. AeroCom multiple-dust
71 model intercomparison was performed on both global and regional scales (Huneeus et al.,
72 2011) but only focused on one year, thus models' capability of simulating interannual or
73 long-term variability of dust is not clear. A comprehensive evaluation of the climatology
74 and interannual variation of global dust optical depth (DOD) in CMIP5 models will
75 provide a clear picture of model capability of dust simulation.

76 Here we examine the results of seven CMIP5 models (Table 1) by comparing
77 model output with DOD derived from Moderate Resolution Imaging Spectroradiometer
78 (MODIS) Deep Blue aerosol products. Projections on changes of DOD in the late half of
79 the 21st century by CMIP5 models and also by a regression model (Pu and Ginoux, 2017)
80 are examined and analyzed.

81 The following section introduces data and methods used in this study. Results are
82 presented in section 3, including examinations on the climatology and interannual
83 variations of modeled DOD and future projections. Discussion and major conclusions are
84 presented in sections 4 and 5, respectively.

85

86 **2. Data and Methodology**

87 **2.1 DOD from MODIS**

88 DOD is a widely used variable that describes optical depth due to the extinction
89 by mineral particles. It is one of the key factors (single scattering albedo and asymmetry
90 factor being the two others) controlling dust interaction with radiation. Monthly DOD are



91 derived from MODIS aerosol products retrieved using the Deep Blue (MDB2) algorithm,
92 which employs radiance from the blue channels to detect aerosols globally over land even
93 over bright surfaces, such as desert (Hsu et al., 2004, 2006). Ginoux et al. (2012b) used
94 collection 5.1 level 2 aerosol products from MODIS aboard the Aqua satellite to derive
95 DOD. Here, both MODIS aerosol products (collection 6, level 2; Levy et al., 2013) from
96 the Aqua and Terra platforms are used. Aerosol products such as AOD, single scattering
97 albedo, and the Ångström exponent are first interpolated to a regular 0.1° by 0.1° grid
98 using the algorithm described by Ginoux et al. (2010). The DOD is then derived from
99 AOD following the methods of Ginoux et al. (2012b) with adaptations for the newly
100 released MODIS collection 6 aerosol products (Pu and Ginoux, 2016).

101 Daily DOD is derived for both Aqua and Terra satellites and then averaged to
102 monthly data and interpolated to a 1° by 1° grid. Terra passes the Equator from north to
103 south around 10:30 local time while Aqua passes the Equator from south to north around
104 13:30 local time. To reduce missing data and also to combine the information from both
105 morning and afternoon hours, a combined monthly DOD (here after MODIS DOD) is
106 derived by averaging Aqua and Terra DOD when both products exist or using either
107 Aqua or Terra DOD when only one product is available. As shown in Figure S1 in the
108 Supplement, the mean available days in each season and also spatial coverage are
109 enhanced in combined DOD than using Aqua or Terra (not shown) DOD alone. This
110 combined DOD is available from January 2003 to December 2016.

111 Aqua and Terra DOD product has previously been used to study global dust
112 sources (Ginoux et al., 2012b), dust variations in the Middle East (Pu and Ginoux, 2016)
113 and the U.S. (Pu and Ginoux, 2017), and has been validated with Aerosol Robotic



114 NETWORK (AERONET) stations over the U.S. (Pu and Ginoux, 2017). Here we compared
115 MODIS DOD climatology with both AERONET observation and DOD retrieved from
116 Cloud-Aerosol Lidar with Orthogonal Polarization (CALIOP; Winker et al., 2004; 2007)
117 aboard the Cloud-Aerosol Lidar and Infrared Pathfinder Satellite Observation
118 (CALIPSO) satellite. AERONET stations provide cloud-screened and quality assured
119 (level 2) coarse mode aerosol optical depth (COD) at 500 nm, which is processed by the
120 Spectral Deconvolution Algorithm (O'Neill et al., 2003). Only nine sites have COD
121 records during 2003-2016, and the climatological mean of MODIS DOD generally
122 compares well with these sites (Figure S2 in the Supplement).

123 CALIOP measures backscattered radiances attenuated by the presence of aerosols
124 and clouds and retrieves corresponding microphysical and optical properties of aerosols.
125 Monthly dust AOD (or DOD) on a 2° latitude by 5° longitude grid are available since
126 June 2006. The climatology of CALIOP DOD during 2007-2016 is similar to that of
127 MODIS DOD during the same period (Figure S3 in the Supplement). The global mean
128 (over land) MODIS DOD is slightly higher than that from CALIOP, probably due to the
129 lower horizontal resolution of the latter. The pattern correlations (e.g., Pu et al., 2016)
130 between the two products range from 0.83 in boreal spring and summer to 0.63 in boreal
131 winter (Figure S3 in the Supplement).

132 Due to higher spatial resolution (compared with CALIOP) and coverage
133 (compared with AERONET sites), MODIS DOD is chosen as the primary product to
134 validate CMIP5 model output. Nine regions (Table 2) are selected to study the DOD
135 magnitude, spatial pattern, and variations. These regions cover major dust source regions
136 previously identified (Ginoux et al. 2012).



137 2.2 Reanalysis and observation datasets

138 To examine the interannual variations of DOD and its connection with local
139 controlling factors such as surface wind speed, bareness, and precipitation, monthly data
140 of 10 m wind speed from the ERA-Interim (Dee et al., 2011), leaf area index (LAI) data
141 from Advanced Very High Resolution Radiometer (AVHRR; Claverie et al., 2014,
142 2016), and precipitation from the Precipitation Reconstruction over Land (PRECL; Chen
143 et al., 2002) are used.

144 ERA-Interim is a global reanalysis from the European Centre for Medium-Range
145 Weather Forecasts (ECMWF). Its horizontal resolution is T255 (about 0.75° or 80 km),
146 very suitable to study the influence of wind speed on dust emission and transport on
147 small scales. The monthly data are available from 1979 to present day.

148 Monthly LAI derived from the version 4 of Climate Data Record (CDR) of
149 AVHRR is used to calculate surface bareness. The data are produced by the National
150 Aeronautics and Space Administration (NASA) Goddard Space Flight Center (GSFC)
151 and the University of Maryland. Monthly gridded data on a horizontal resolution of 0.05°
152 by 0.05° degree are available from 1981 to present. This product is selected due to its
153 high spatial resolution and long temporal coverage. Surface bareness is calculated from
154 seasonal mean LAI as the following,

$$155 \quad \text{Bareness} = \exp(-1 \times \text{LAI}) \quad (1)$$

156 PRECL precipitation from the National Oceanic and Atmospheric Administration
157 (NOAA) is a global analysis available monthly from 1948 to present at a 1° by 1°
158 resolution. The dataset is derived from gauge observations from the Global Historical
159 Climatology Network (GHCN), version 2, and the Climate Anomaly Monitoring System



160 (CAM5) datasets. Its long coverage and relatively high spatial resolution is quite suitable
161 to study the connections between DOD and precipitation.

162

163 **2.3 CMIP5 model output**

164 Among CMIP5 models we selected seven models that used interactive dust
165 emission schemes, in which dust emission varied in response to changes of climate. The
166 output of 10 m wind speed, precipitation, and LAI are also available from these models.
167 Other models (to our best knowledge) either used offline dust as an input, in which dust
168 emission did not interactively respond to meteorological and climate changes, or did not
169 write out the variables needed for this analysis.

170 Both historical run from 1861 to 2005 and future run under the Representative
171 Concentration Pathways 8.5 (RCP 8.5) scenario (Riahi et al., 2011) from 2006 to 2100
172 are used. Here the RCP 8.5 scenario is chosen because it represents the upper limit of the
173 projected greenhouse gas change in the twenty-first century and thus likely is the worst-
174 case scenario for future DOD variation under climate change. Also, studies found that
175 observed CO₂ emission pathway during 2005-2014 matches RCP 8.5 scenario better than
176 other scenarios (e.g., Fuss et al., 2014), which makes the RCP8.5 output suitable to
177 examine present-day DOD variations after 2005.

178 Monthly model output of dust load, surface 10 m wind speed, precipitation, and
179 LAI are used. Historical output from 2003 to 2005 and RCP 8.5 output from 2006 to
180 2016 are combined to form time series and climatology during 2003-2016 to compare
181 with MODIS DOD during the same time period.

182



183 **2.3.1 DOD derived from modeled dust load**

184 Most CMIP5 models did not save DOD, so we used monthly dust load and
185 converted them to DOD using the relationship derived by Ginoux et al. (2012a) as the
186 following

$$187 \quad \tau = M \times e, \quad (2)$$

188 where τ is DOD at 500 nm, M is the load of dust in unit of (g m^{-2}), and $e = 0.6 \text{ m}^2 \text{ g}^{-1}$ is
189 the mass extinction efficiency. Dust load from different models is first interpolated to a
190 2° by 2.5° grid and then converted to DOD. The same method was used by Pu and
191 Ginoux (2017) for the U.S. We compared the derived DOD with modeled DOD from one
192 historical simulation of GFLD-CM3 model (Donner et al., 2011). The pattern correlation
193 of the climatology (1861-2005) between the derived DOD and modeled DOD are very
194 high, all above 0.99 for four seasons (not shown). The percentage differences between
195 derived DOD and modeled DOD averaged over global land range from -3.6% in DJF and
196 SON to 1.3% in MAM and JJA. Over Africa, DOD is slightly overestimated by 0~6.7%
197 (regional mean), while over the Middle East, there is a small underestimation by -1.6% in
198 SON and up to 8.2% overestimation in JJA. Among the nine regions we focused in this
199 analysis, three regions (North America, South Africa, and South America) show an
200 underestimation of more than 20% in some seasons and two regions (Northern China and
201 Australia) show an overestimation of more than 10% in some seasons.

202

203 **2.4 Multiple linear regression**

204 In order to examine the relative contribution of each local controlling factor to
205 DOD variations, multiple linear regression is applied by regressing DOD onto



206 standardized seasonal mean ERA-Interim surface wind speed, AVHRR bareness, and
207 PRECL precipitation at each grid point. All the data are re-gridded to a 1° by 1° grid
208 before the calculation. Over regions where values are missing for any of the explanatory
209 variables (i.e., precipitation, bareness, and surface wind speed) or DOD, the regression
210 coefficients are set to missing values. The collinearity among these explanatory variables
211 is examined by calculating variance inflation factor (VIF) (e.g., O'Brien, 2007; Abudu et
212 al., 2011), and in most regions the VIF is below 2 (not shown), indicating a low
213 collinearity (5–10 is usually considered high). Bootstrap resampling is used to test the
214 significance of the regression coefficients, following the method used by Pu and Ginoux
215 (2017).

216 Multiple linear regression is also applied to CMIP5 model derived DOD and
217 output of surface wind speed, bareness, and precipitation to obtain regression coefficients
218 from the models. All variables are interpolated to a 2° by 2.5° grid before regression.
219 The results are compared with regression coefficients derived from observational
220 datasets.

221 Similar to the method used by Pu and Ginoux (2017), the regression coefficients
222 derived from MODIS DOD and observed controlling factors from 2004 to 2016 and
223 CMIP5 model output of surface wind speed, bareness, and precipitation are used to
224 project variations of future DOD. Here we tried two groups of CMIP5 output for these
225 controlling factors. One group used seven models with interactive dust emission scheme
226 (Table 1), and the other used 16 CMIP5 models as did by Pu and Ginoux (2017; their
227 Supplementary Table S1). The reason to test the latter is to include as much model output
228 of the controlling factors as possible. The differences between the historical run (1861–



229 2005 average) and that of the RCP 8.5 run for the late half of the twenty-first century
230 (2051–2100) are standardized by the standard deviation of the historical run for each
231 explanatory variable. The projected change reveals how DOD will vary with reference to
232 the historical conditions (mean and standard deviation).

233

234 **3. Results**

235 **3.1 Climatology (2004-2016)**

236 Figure 1 shows the climatology of MODIS DOD (top panel) in four seasons
237 during 2004-2016 and that from the CMIP5 multi-model mean (bottom). Globally, the
238 dustiest regions are largely located over the northern hemisphere (NH) over North Africa,
239 the Middle East, and East Asia (Figs. 1a-d). In these regions, DOD is higher in boreal
240 spring and summer than fall and winter. Modeled global DOD over land is generally
241 lower than that from MODIS DOD, ranging from -0.028 (-25.2%) in MAM to -0.005 (-
242 6.4%) in DJF. The global spatial pattern is better captured in MAM and JJA, with pattern
243 correlations of 0.74 and 0.85, respectively (Figs. 1f-g). In DJF, DOD is overestimated
244 over central Africa and Australia, but underestimated over the Middle East and Asia (Fig.
245 1e), while in SON there is a similar overestimation in Australia and an underestimation in
246 the Middle East (Fig. 1h).

247 Figure 2 shows the zonal mean of CMIP5 DOD from individual models (thin
248 colorful lines) and multi-model ensemble mean (thick black), in comparison with MODIS
249 DOD (thick red). In DJF, DOD is underestimated in the NH from 15° N to 50°N but
250 overestimated over the tropics and southern hemisphere (SH) (Fig. 2a). While the
251 overestimation in the SH is largely contributed by three models, the underestimation in



252 the NH appears in all the seven models. The overestimation of DOD in HadGEM2-ES
253 has also been identified in a previous study (Bellouin et al., 2011) and will be discussed
254 later. In MAM, a similar overestimation of DOD in the tropics and SH also occurs in
255 some models, and the multi-model mean slightly overestimates DOD around 20°-30°S
256 (Fig. 2b). In NH, there is a weak underestimation too, but the overall gradient is largely
257 captured. In JJA, the multi-model mean resembles MODIS DOD very well (Fig. 2c),
258 consistent with the highest pattern correlation in this season shown in Fig. 1. The peak
259 around 19° N in North Africa and Middle East is well captured by the multi-model mean,
260 although the magnitude is slightly underestimated. In SON, different from MODIS DOD
261 that peaks around 19°N, the multi-model mean has two peaks around 15°N and 28°S,
262 respectively, a pattern somewhat similar to that in DJF (Fig. 2d). Consequently, DOD in
263 CMIP5 multi-model mean is overestimated at 15°-40°S and 0°-15°N but underestimated
264 at 15°S -0° and 15°-40°N.

265 Seasonal cycles of CMIP5 DOD are compared with MODIS DOD in nine regions
266 in Figure 3. The annual means of DOD in each region from multi-model mean (black)
267 and MODIS (red) are also listed in each plot. The spread of DOD among individual
268 models is greater during boreal spring and summer for regions in the NH and during
269 austral spring and summer for regions in the SH than other seasons. Seasonal cycles over
270 North Africa, the Middle East, North America and India are generally captured, with
271 modeled DOD peaking during the same seasons as MODIS DOD. Over northern China,
272 MODIS DOD peaks in spring, consistent with previous studies (e.g., Zhao et al., 2006;
273 Laurent et al., 2006; Ginoux et al., 2012b), while multi-model mean peaks much later in
274 June. Similar misrepresentation occurs over the southeastern Asia. In South Africa and



275 South America the observed maxima in early austral spring (i.e., September) are also
276 missed. In Australia, DOD is largely overestimated and the peak from November to
277 January in MODIS DOD is also misrepresented in the multi-model mean. Similar to the
278 finding here, Bellouin et al. (2011) also found that HadGEM2-ES model overestimated
279 DOD over Australia and Thar desert region in northwestern India and suggested that
280 these overestimations were likely due to model's overestimation of bare soil fraction and
281 underestimation of soil moisture.

282 We further examine the magnitudes and spatial patterns of CMIP5 DOD in these
283 regions. Figure 4 shows the ratio of pattern standard deviations (standard deviations of
284 values within the domain) and pattern correlation between CMIP5 DOD and MODIS
285 DOD climatology (2004-2016) in each region for four seasons. While the former reveals
286 the magnitude differences, the latter demonstrates the spatial resemblance.

287 Over North Africa, the Middle East, and India, the ratio of CMIP5 DOD from
288 individual models and multi-model mean versus MODIS DOD are all within \pm one order
289 of magnitude (Fig. 4). Most models underestimate DOD in northern China, although the
290 magnitudes are largely within the range of -one order of magnitude to one. Over North
291 America, South Africa, and Australia, some models underestimate the DOD by more than
292 two orders of magnitudes, while over Australia three models overestimate DOD by more
293 than one order of magnitude. In general, magnitudes of multi-model mean are closer to
294 satellite DOD than most individual models and are largely within \pm one order of
295 magnitude of MODIS DOD.

296 The spatial patterns are better captured over North Africa and the Middle East
297 than other regions (Fig. 4), with pattern correlations above 0.6 in most models (with



298 highest pattern correlation of 0.92 and 0.83, respectively). Pattern correlations from
299 multi-model mean are also high, reaching 0.87 (0.78) over North Africa and 0.75 (0.73)
300 over the Middle East in JJA (MAM). Nonetheless, some models show negative pattern
301 correlations over North Africa, northern China, North America, southeastern Asia, South
302 Africa, South America, and Australia. Overall, spatial patterns are less well represented
303 in regions over the SH than over the NH in CMIP5 models.

304 In short, in terms of both magnitudes and spatial pattern, DOD climatology is best
305 represented over North Africa and the Middle East among the nine regions. The multi-
306 model mean shows that DOD over North Africa is slightly better simulated than over the
307 Middle East, somewhat similar to the finding of AeroCom multi-model analysis
308 (Huneus et al. 2011).

309

310 **3.2 Interannual variations**

311 An important aspect of dust activity is its long-term variations, including
312 interannual and decadal variations. Dust emission in North Africa is known to have
313 strong decadal variations (e.g., Prospero and Nees, 1986; Prospero and Lamb, 2003;
314 Mahowald et al., 2010; Evan et al., 2014, 2016), while over Australia, strong interannual
315 variations have been related to El Niño–Southern Oscillation (e.g., Marx et al., 2009;
316 Evans et al., 2016). Due to the short time coverage of high quality satellite products, we
317 focus on interannual variations of DOD from 2004 to 2016.

318 Figure 5 shows the correlations of regional mean time series of DOD between
319 MODIS and CMIP5 models and multi-model mean for each season in nine regions. We
320 also show correlations between the reconstructed DOD and MODIS DOD for reference



321 (Table S1 in the Supplement). Previous study found that the variations of dust event
322 frequency over the U.S. in the recent decade could be largely represented by the
323 variations of three local controlling factors: seasonal mean surface wind speed, bareness,
324 and precipitation (Pu and Ginoux, 2017). These factors have previously been found to
325 constrain dust emission or variability on multiple time scales (e.g., Gillette and Passi,
326 1988; Fecan et al., 1999; Zender and Kwon, 2005). While surface wind is positively
327 related to the emission and transport of dust, vegetation is an important non-erodible
328 element that prevents soil erosion from wind. Precipitation is generally negatively related
329 to dust emission and transport processes. While the scavenging effect of precipitation on
330 small dust particles only lasts a few hours or days, influences of precipitation on soil
331 moisture lasts longer. Here we extend our regression model (Pu and Ginoux, 2017) to a
332 global scale. Regression coefficients are obtained by regressing MODIS DOD onto
333 observed surface wind, bareness, and precipitation during 2004-2016 (see methodology
334 section for details). The reconstructed DOD is then calculated using these regression
335 coefficients and time-varying controlling factors.

336 The interannual variations of DOD are in general not well captured by CMIP5
337 models. This is consistent with previous study by Evan et al. (2014) who found dust
338 variability downwind of North Africa over the northeastern Atlantic was misrepresented
339 in CMIP5 models. In most regions, only one or two models show significant positive
340 correlation with MODIS DOD in some seasons, and negative correlations exist in all
341 regions (Fig. 5). North Africa, the Middle East, southeastern Asia, South America, and
342 Australia show less negative correlations than other dusty regions. On the other hand,
343 reconstructed DOD shows significant positive correlations with MODIS DOD over most



344 regions in all seasons (Table S1 in the Supplement). This suggests that the interannual
345 variations of DOD can be largely attributed to the variations of these controlling factors,
346 and models probably misrepresented these relationships, in addition to their incapacity of
347 capturing the interannual variations of individual controlling factors in general (Figures
348 S4-6 in the Supplement), which is not uncommon for coupled models.

349 We further examine the connection between those controlling factors and DOD in
350 CMIP5 models. Figure 6 shows the dominant controlling factors among the three (surface
351 wind speed, bareness, and precipitation) on DOD variations in four seasons from MODIS
352 (left column) and from CMIP5 multi-model mean (right column), respectively. To
353 highlight factors controlling DOD variations near the dust source regions, a mask of
354 AVHRR LAI \leq 0.5 is applied to both coefficients.

355 Bareness plays the most important role in many dusty regions in observations,
356 e.g., over Australia, central U.S., and South America (Figs. 6a-d). Note that while
357 bareness plays an important role over the Sahel during DJF and MAM, it also shows
358 strong signal over some areas in the northern North Africa (Figs. 6a-b). The reliability of
359 this information is limited by the accuracy of LAI retrieval in these areas. The value of
360 bareness in this region is actually quite high (as LAI is very low), but still has weak
361 interannual variability (Figures S7 in the Supplement). Over some areas of North and
362 South Africa, the Middle East, and East Asia, surface wind and precipitation are also
363 quite important.

364 The role of bareness is largely underestimated in CMIP5 models, while surface
365 wind and precipitation become the dominant factors (Figs. 6e-h). The misrepresentation
366 of the connection between DOD and these controlling factors may cause the



367 misrepresentation of the dust load and its variability. Taking Australia for an example,
368 the overestimation of DOD magnitudes may be related to an overestimation of the
369 influence of surface wind on DOD and a lack of constraints from surface bareness.

370 Despite the large differences between the observed and modeled connections
371 between DOD and the controlling factors, some regions show similarities. For instance,
372 over North Africa in DJF, both show an important influence from surface winds (Figs.
373 6a, e), although the locations of surface wind-dominant areas are not exactly the same.
374 Evan et al. (2016) also found a dominant role of surface wind on African dust variability,
375 but they focused on monthly means, not seasonal averages. In MAM, precipitation starts
376 to play a role in some parts of North Africa, while surface wind still dominates in some
377 areas (Fig. 6b). Same increasing influence of precipitation is shown in the multi-model
378 mean, but such an influence seems overestimated (Fig. 6f). In JJA, the influences of
379 surface wind in North Africa and precipitation and bareness in the Middle East in the
380 multi-model mean (Fig. 6g) also show some similarity to observation (Fig. 6c), although
381 an underestimation of the influence from bareness and an overestimation of surface wind
382 are still there.

383 Also, note that in CMIP5 models, due to lack of constraints from low surface
384 temperature (e.g., over frozen land) and snow cover on dust emission or
385 misrepresentations of dust transport, DOD and also the regression coefficients still exist
386 over NH high latitudes in boreal winter and spring in the multi-model mean (Figs. 6e-f).

387

388

389



390 **3.3 Future projections**

391 How will DOD change in response to increasing greenhouse gases? The results
392 from CMIP5 multi-model mean are shown in Figure 7. We compare the DOD during the
393 late half of the 21st century under the RCP 8.5 scenario with that in the historical level
394 (1861-2005 average).

395 Over land, CMIP5 model projects a decrease of global mean DOD in all seasons
396 except JJA (Figs. 7a-d). The inter-model standard deviation is much greater than the
397 multi-model mean, suggesting large discrepancies among individual models. The
398 projected decrease is largely over northern North America, southern North Africa, eastern
399 central Africa, and East Asia, while the increase is largely over northern North Africa, the
400 Middle East, southern North America, South Africa, South America, and southern
401 Australia (Fig. 7). Regional means of DOD change (in percentage) with reference to
402 CMIP5 historical run are summarized in Table 3.

403 What might be the causes of DOD change? Figure 8 shows the projected change
404 of precipitation, bareness, and surface wind speed from CMIP5 multi-model mean. These
405 factors play important role in DOD variations in the present day, although models tend to
406 underestimate the role of bareness and overestimate the influences of precipitation and
407 surface wind (Fig. 6). Increases in precipitation can increase soil moisture and remove
408 airborne dust, thus usually favors a decrease of DOD. As shown in Figs. 8a-d, the
409 increases of precipitation in northern Eurasia, northern North America, the Congo basin
410 in Africa, and Australia (DJF and MAM) may contribute to the decrease of DOD in these
411 regions, while the decreases of precipitation over northern North Africa and the Middle
412 East (DJF and MAM), South Africa, and South America may contribute to the increase of



413 DOD (DJF-SON). Also note that in JJA both precipitation and DOD increase over
414 northern North Africa and the Middle East (Fig. 8c), suggesting other factors dominate
415 the variation of DOD in the multi-model mean.

416 A decrease (increase) of bareness indicates a growth (decay) of vegetation and is
417 usually associated with a decrease (increase) of DOD. In general, except regions such as
418 southern North America, South America, South Africa, part of northern Eurasia, and
419 central Sahel, the pattern of bareness change does not resemble DOD change (Figs. 8e-h).
420 This is probably due to the fact that the overall influence of bareness on DOD variation is
421 underestimated in CMIP5 models (Fig. 6).

422 Increases in surface wind can enhance dust emission and transport, and vice versa.
423 The changes of surface wind in DJF and MAM are similar and likely to contribute to the
424 increase of DOD over northern North Africa, the Middle East, eastern South America,
425 southern South Africa, southern Australia (Figs. 8i-j). The decrease of DOD over
426 northwestern North America, the Sahel, and northern Australia may also relate to the
427 decrease of surface wind there, in addition to an increase of precipitation and a reduction
428 of bareness. In JJA and SON (Figs. 8k-l), the increases of surface wind in South America,
429 South Africa, central Australia and the decreases of wind in northwestern North America,
430 northern Eurasia, and the central Sahel are also consistent with patterns of DOD change.

431 In short, variations of CMIP5 DOD in the late half of the 21st century are more
432 consistent with changes of precipitation and surface wind speed than with surface
433 bareness, consistent with the analysis above regarding to the present-day condition.

434 The projected change of DOD from the regression model is shown Figure 9. The
435 results are calculated using the regression coefficients obtained from observations during



436 2004-2016 and projected changes of precipitation, bareness, and surface wind speed from
437 16 CMIP5 models (see methodology). A similar method is applied to the model output
438 from seven CMIP5 models with interactive dust emission scheme, and results are similar
439 (Figure S8 in the Supplement) A mask of present-day LAI ≤ 0.5 is also applied to
440 highlight the changes of DOD near dust source regions. By doing this, we assume the
441 location of major dust sources will not change much at the late half of the 21st century.
442 The unmasked figure is presented in the supplementary file (Figure S9 in the
443 Supplement). The reason we did not use the projected future LAI as a mask is that
444 there're large uncertainties associated with LAI projection, especially over northern
445 hemisphere subtropical regions (e.g., Figs. 8e-h).

446 In DJF, regression model projected change of DOD over Mexico, North Africa,
447 the Middle East and part of northern China (Fig. 9a) are similar to those projected by
448 CMIP5 models over those dust source regions (Fig. 7a), but with a greater magnitude. In
449 MAM, a decrease of DOD is projected over large area of North Africa (Fig. 9b), which is
450 different from the pattern projected from the CMIP5 multi-model mean (Fig. 7b). The
451 decrease of DOD over northern central U.S. is also different from the overall increase
452 projected by CMIP5 DOD, as also noted by Pu and Ginoux (2017). However, the
453 increase of DOD over the Middle East and the decrease of DOD over northern China are
454 similar to that of CMIP5 DOD. During JJA and SON, DOD decreases over the Sahel and
455 northern China but increases over a belt to the north of central Sahel and parts of the
456 Middle East (Figs. 9c-d). The weak increase of DOD over the southern corner of South
457 Africa in JJA and a slight decrease in SON also has high agreement among the models.



458 Changes of DOD over Australia are very small and show little consistency among the
459 models.

460 The contribution of each controlling factor to the total DOD change is shown in
461 Figure 10. While changes of bareness over North Africa, northern Middle East and
462 northern China play an important role in DOD change, changes of precipitation, e.g. over
463 northwestern China in MAM, and surface wind, e.g., over North Africa and the Middle
464 East in DJF and MAM, also play vital roles.

465 Both projections from the CMIP5 models and that from the regression model have
466 large uncertainties. The reliability of future projection by CMIP5 models is limited by
467 models' capability of capturing present-day climatology and observed connection
468 between DOD and local controlling factors. As discussed earlier, the overall performance
469 of models is better in those very dusty regions in the NH, such as North Africa and the
470 Middle East, than other regions. Multi-model mean also overestimates the connection
471 between DOD and precipitation and surface wind and underestimates the influence of
472 bareness, which can cast doubts on the projected variation of DOD in response to climate
473 change.

474 The uncertainties associated with regression model are two folds. First, there're
475 uncertainties associated with the regression model itself. Since the regression coefficients
476 are derived from observed relationships between DOD and controlling factors in a
477 relatively short time period, factors controlling the low frequency variation of DOD (e.g.,
478 decadal variations) may not be included. Other meteorological factors that could play an
479 important role in regional dust variability, e.g., nocturnal low-level jets (e.g., Todd et al.,
480 2008; Fiedler et al., 2013; Fiedler et al., 2016) and haboobs over Africa (e.g., Ashpole



481 and Washington, 2013), are not directly considered in the model. The influences of
482 anthropogenic land use/land cover change are also not included in the regression model.
483 Anthropogenic land use/land cover change has been found to have played an important
484 role in long-term dust variability in some regions (e.g., Neff et al., 2005; 2008; Moulin
485 and Chiapello, 2006; McConnell et al., 2007), although previous modeling study found
486 its influences on future dust emission was minor compared to climate change (Tegen et
487 al., 2004). So the projection made by the regression model only reveals the change of
488 DOD in association with climate change. Second, uncertainties associated with model
489 projected change of controlling factors, such as bareness in U.S. in JJA as pointed by Pu
490 and Ginoux (2017), also limit the accuracy of the results.

491 Despite these uncertainties, both methods make similar projections particularly in
492 some dusty regions. For instance, the DOD pattern over North Africa in DJF and JJA, an
493 increase of DOD in the Arabian Peninsula in all seasons, and a decrease of DOD over
494 northern China from MAM to SON (Figs. 7, 9).

495

496 **4. Discussion**

497 We examined DOD in seven CMIP5 models with interactive dust emission
498 schemes. Other important variables that influence the radiative property and
499 concentration of dust, such as Angström exponent, dust emission, and surface
500 concentration, are worth further examination, if these variables are archived. A better
501 quantification of the radiative forcing of dust may also require an examination on the size
502 distribution of dust particles, as studies (e.g., Kok et al., 2017) found in current AeroCom



503 models fraction of coarse dust particles were underestimated and so was the warming
504 effect of dust. Whether this is the case in the CMIP5 models is not clear.

505 Early studies on future dust projection used offline dust models driven by climate
506 model output under different scenarios. For instance, Mahowald and Luo (2003) used an
507 offline dust model and output from National Center of Atmospheric Research's coupled
508 Climate System Model (CSM) 1.0 (Boville and Gent, 1998) under A1 scenario
509 (Houghton et al., 2001) and projected a decrease of dust emission by the end of the 21st
510 century by -20% to -63%, depending on different scenarios. In general, when they
511 included vegetation change, the projected dust reduction became greater, but including
512 land use change slightly weakened such reduction. Similarly, Tegen et al. (2004) used
513 output from ECHAM4 and HadCM3 and a dust model (Tegen et al., 2002) to examine
514 the change of dust emission by 2040-2050 and 2070-2080 and found results were model
515 and scenario dependent, from -26% to 10%. However, including anthropogenic
516 cultivation practices tended to increase dust emission in both models. They also pointed
517 out that such an influence from anthropogenic land-use was not big enough to overcome
518 the effect of climate change.

519 The interactive dust emission schemes and new generations of climate models
520 used in CMIP5 are likely to provide more reliable projections, but this may also depend
521 on how changes of dust and its radiative forcing are fed back to the climate system in the
522 models. While these projections are largely model-dependent, based on our analysis on
523 the DOD climatology in CMIP5 models, the multi-model mean has a better chance to
524 provide a more reliable projection than individual models.



525 Here a regression model combined with MODIS DOD is used to identify key
526 local factors that control the variation of DOD on the interannual time scale. The results
527 are then compared with model output to examine models' capability of capturing
528 observed connections between DOD and controlling factors. This method may be applied
529 to other dust model intercomparison projects as well, such as AeroCom (Huneeus et al.
530 2011), to help examine model performance.

531

532 **5. Conclusion**

533 Dust aerosol plays an important role in the climate system by directly scattering
534 and absorbing solar and longwave radiation and indirectly affecting the formation and
535 radiative properties of cloud. It is thus very important to understand how well dust is
536 simulated in the state-of-the-art climate models. While many features and variables are
537 systematically examined in the CMIP5 multi-model output, we found that to our best
538 knowledge an evaluation of global dust modeling in CMIP5 models is still in blank. In
539 this study we examined a key variable associated with dust radiative effect, dust optical
540 depth (DOD), using seven CMIP5 models with interactive dust emission schemes and
541 DOD retrieved from MODIS Deep Blue aerosol products.

542 We found that the global spatial pattern and magnitude are largely captured by
543 CMIP5 models in the 2004-2016 climatology, with an underestimation of global DOD
544 (over land) by -25.2% in MAM to -6.4% in DJF. The spatial pattern is better captured in
545 boreal dusty seasons during MAM and JJA. In JJA, the simulated zonal mean DOD from
546 multi-model mean captures MODIS DOD quite well.



547 The magnitudes of multi-model mean are closer to MODIS climatology than most
548 individual models and are largely within \pm one order of magnitude of MODIS DOD in
549 the nine regions examined here (North Africa, the Middle East, Northern China, North
550 America, India, southeastern Asia, South Africa, South America, and Australia; see Fig. 1
551 and Table 2 for domains). While some models underestimate DOD in North America and
552 South America by more than two orders of magnitude, a few also overestimate DOD in
553 Australia by more than one order of magnitude. Both the magnitude and spatial patterns
554 of DOD are better captured over North Africa and the Middle East than other regions.

555 The multi-model mean also largely captures the seasonal cycle of DOD in some
556 very dusty regions, such as North Africa and the Middle East. Seasonal variations in
557 North America and India are also generally captured, with the modeled DOD peaking at
558 approximately the same season as in MODIS DOD, but not so in Northern China and
559 southeastern Asia. Seasonal cycles in those dusty regions in the southern hemisphere is
560 generally not well captured, with modeled DOD over South Africa and South America
561 peaking later than that in MODIS DOD but earlier in Australia.

562 The interannual variations of DOD are not captured by most of the CMIP5
563 models during 2004-2016. This is likely due to models' underestimation of the
564 constraints from surface bareness on dust and overestimation of the influences from
565 surface wind speed and precipitation in those major dust source regions, in addition to the
566 fact that coupled models usually do not capture the observed interannual variations of
567 precipitation, surface wind, and bareness as well. CMIP5 model projected change of
568 DOD in the late half of the 21st century (under the RCP 8.5 scenario) with reference to
569 historical condition (1861-2005) also shows greater influence from precipitation and



570 surface wind change than from surface bareness. Overall, multi-model mean projects a
571 change of DOD over land from -3.8% in SON to 3.3% in JJA.

572 We also provide a projection of future DOD change using a regression model
573 based on local controlling factors such as surface wind, bareness, and precipitation (Pu
574 and Ginoux, 2017). This model can largely capture the interannual variations of DOD in
575 2004-2016. The regression model projects a reduction of DOD in the Sahel in all seasons
576 in the late half of the 21st century under the RCP 8.5 scenario, largely due to a decrease of
577 surface bareness. DOD is projected to increase over the southern edge of Sahara in
578 association with surface wind and precipitation changes except in MAM, when a
579 reduction of DOD over most part of North Africa is projected. DOD is also projected to
580 increase over the Arabian Peninsula in all seasons and to decrease over northern China
581 from MAM to SON.

582 Despite large uncertainties associated with both projections, we find some
583 similarities between the two, which may be informative, for instance, changes of DOD
584 over North Africa in DJF and JJA, an increase of DOD in the Arabian Peninsula in all
585 seasons, and a decrease of DOD over northern China from MAM to SON.

586

587

588

589

590

591

592



593 *Acknowledgements.*

594 This research is supported by NOAA and Princeton University's Cooperative
595 Institute for Climate Science and NASA under grant NNH14ZDA001N-ACMAP. The
596 authors thank Drs. Songmiao Fan and Fabien Paulot for their helpful comments on the
597 early version of this paper.

598 PRECL Precipitation data are provided by the NOAA/OAR/ESRL PSD, Boulder,
599 Colorado, USA, from their web site at <http://www.esrl.noaa.gov/psd/>. The CALIOP
600 products are downloaded from [https://www-](https://www-calipso.larc.nasa.gov/tools/data_avail/dpo_read.php?y=2007&m=08&d=10)
601 [calipso.larc.nasa.gov/tools/data_avail/dpo_read.php?y=2007&m=08&d=10](https://www-calipso.larc.nasa.gov/tools/data_avail/dpo_read.php?y=2007&m=08&d=10). AVHRR
602 leaf area index data are available at: <ftp://eclipse.ncdc.noaa.gov/pub/cdr/lai-fapar/files/>.
603 The ERA-Interim is downloaded from [http://www.ecmwf.int/en/research/climate-](http://www.ecmwf.int/en/research/climate-reanalysis/era-interim)
604 [reanalysis/era-interim](http://www.ecmwf.int/en/research/climate-reanalysis/era-interim). The AERONET coarse mode aerosol optical depth data are
605 downloaded from <https://aeronet.gsfc.nasa.gov/>. CMIP5 data are downloaded from:
606 <https://pcmdi.llnl.gov/projects/esgf-llnl/>.

607

608

609

610

611

612

613

614

615



- 616 Reference
617
618 Abudu, S., Cui, C. L., King, J. P., Moreno, J., and Bawazir, A. S.: Modeling of daily pan
619 evaporation using partial least squares regression, *Sci China Technol Sc*, 54, 163-
620 174, 10.1007/s11431-010-4205-z, 2011.
- 621 Arora, V. K., Scinocca, J. F., Boer, G. J., Christian, J. R., Denman, K. L., Flato, G. M.,
622 Kharin, V. V., Lee, W. G., and Merryfield, W. J.: Carbon emission limits required
623 to satisfy future representative concentration pathways of greenhouse gases,
624 *Geophys Res Lett*, 38, 10.1029/2010gl046270, 2011.
- 625 Ashpole, I., and Washington, R.: A new high-resolution central and western Saharan
626 summertime dust source map from automated satellite dust plume tracking, *J*
627 *Geophys Res-Atmos*, 118, 6981-6995, 10.1002/jgrd.50554, 2013.
- 628 Bangert, M., Nenes, A., Vogel, B., Vogel, H., Barahona, D., Karydis, V. A., Kumar, P.,
629 Kottmeier, C., and Blahak, U.: Saharan dust event impacts on cloud formation
630 and radiation over Western Europe, *Atmos Chem Phys*, 12, 4045-4063,
631 10.5194/acp-12-4045-2012, 2012.
- 632 Bellouin, N., Rae, J., Jones, A., Johnson, C., Haywood, J., and Boucher, O.: Aerosol
633 forcing in the Climate Model Intercomparison Project (CMIP5) simulations by
634 HadGEM2-ES and the role of ammonium nitrate, *J Geophys Res-Atmos*, 116,
635 10.1029/2011jd016074, 2011.
- 636 Bentsen, M., Bethke, I., Debernard, J. B., Iversen, T., Kirkevåg, A., Seland, O., Drange,
637 H., Roelandt, C., Seierstad, I. A., Hoose, C., and Kristjansson, J. E.: The
638 Norwegian Earth System Model, NorESM1-M - Part 1: Description and basic



- 639 evaluation of the physical climate, *Geosci Model Dev*, 6, 687-720, 10.5194/gmd-
640 6-687-2013, 2013.
- 641 Boville, B. A., and Gent, P. R.: The NCAR Climate System Model, version one, *J*
642 *Climate*, 11, 1115-1130, Doi 10.1175/1520-
643 0442(1998)011<1115:Tncsmv>2.0.Co;2, 1998.
- 644 Chen, M. Y., Xie, P. P., Janowiak, J. E., and Arkin, P. A.: Global land precipitation: A
645 50-yr monthly analysis based on gauge observations, *J Hydrometeorol*, 3, 249-
646 266, Doi 10.1175/1525-7541(2002)003<0249:Glpaym>2.0.Co;2, 2002.
- 647 Claverie, M., Matthews, J. L., Vermote, E. F., and Justice, C. O.: A 30+ Year AVHRR
648 LAI and FAPAR Climate Data Record: Algorithm Description and Validation,
649 *Remote Sens-Basel*, 8, 10.3390/rs8030263, 2016.
- 650 Collins, W. J., Bellouin, N., Doutriaux-Boucher, M., Gedney, N., Halloran, P., Hinton,
651 T., Hughes, J., Jones, C. D., Joshi, M., Liddicoat, S., Martin, G., O'Connor, F.,
652 Rae, J., Senior, C., Sitch, S., Totterdell, I., Wiltshire, A., and Woodward, S.:
653 Development and evaluation of an Earth-System model-HadGEM2, *Geosci*
654 *Model Dev*, 4, 1051-1075, 10.5194/gmd-4-1051-2011, 2011.
- 655 Cook, B. I., Miller, R. L., and Seager, R.: Dust and sea surface temperature forcing of the
656 1930s "Dust Bowl" drought, *Geophys Res Lett*, 35, 10.1029/2008gl033486, 2008.
- 657 Cook, B. I., Miller, R. L., and Seager, R.: Amplification of the North American "Dust
658 Bowl" drought through human-induced land degradation, *P Natl Acad Sci USA*,
659 106, 4997-5001, 10.1073/pnas.0810200106, 2009.



- 660 Cook, B. I., Seager, R., Miller, R. L., and Mason, J. A.: Intensification of North
661 American Megadroughts through Surface and Dust Aerosol Forcing, *J Climate*,
662 26, 4414-4430, 10.1175/Jcli-D-12-00022.1, 2013.
- 663 Croft, B., Lohmann, U., and von Salzen, K.: Black carbon ageing in the Canadian Centre
664 for Climate modelling and analysis atmospheric general circulation model, *Atmos*
665 *Chem Phys*, 5, 1931-1949, 2005.
- 666 Donner, L. J., Wyman, B. L., Hemler, R. S., Horowitz, L. W., Ming, Y., Zhao, M., Golaz,
667 J. C., Ginoux, P., Lin, S. J., Schwarzkopf, M. D., Austin, J., Alaka, G., Cooke, W.
668 F., Delworth, T. L., Freidenreich, S. M., Gordon, C. T., Griffies, S. M., Held, I.
669 M., Hurlin, W. J., Klein, S. A., Knutson, T. R., Langenhorst, A. R., Lee, H. C.,
670 Lin, Y. L., Magi, B. I., Malyshev, S. L., Milly, P. C. D., Naik, V., Nath, M. J.,
671 Pincus, R., Ploshay, J. J., Ramaswamy, V., Seman, C. J., Shevliakova, E., Sirutis,
672 J. J., Stern, W. F., Stouffer, R. J., Wilson, R. J., Winton, M., Wittenberg, A. T.,
673 and Zeng, F. R.: The Dynamical Core, Physical Parameterizations, and Basic
674 Simulation Characteristics of the Atmospheric Component AM3 of the GFDL
675 Global Coupled Model CM3, *J Climate*, 24, 3484-3519, 10.1175/2011jcli3955.1,
676 2011.
- 677 Dunion, J. P., and Velden, C. S.: The impact of the Saharan air layer on Atlantic tropical
678 cyclone activity, *B Am Meteorol Soc*, 85, 353-+, 10.1175/Bams-85-3-353, 2004.
- 679 Evan, A. T., Dunion, J., Foley, J. A., Heidinger, A. K., and Velden, C. S.: New evidence
680 for a relationship between Atlantic tropical cyclone activity and African dust
681 outbreaks, *Geophys Res Lett*, 33, 10.1029/2006gl026408, 2006.



- 682 Evan, A. T., and Mukhopadhyay, S.: African Dust over the Northern Tropical Atlantic:
683 1955-2008, *J Appl Meteorol Clim*, 49, 2213-2229, 10.1175/2010jamc2485.1,
684 2010.
- 685 Evan, A. T., Flamant, C., Fiedler, S., and Doherty, O.: An analysis of aeolian dust in
686 climate models, *Geophys Res Lett*, 41, 5996-6001, 10.1002/2014gl060545, 2014.
- 687 Evan, A. T., Flamant, C., Gaetani, M., and Guichard, F.: The past, present and future of
688 African dust, *Nature*, 531, 493-+, 10.1038/nature17149, 2016.
- 689 Evans, S., Ginoux, P., Malyshev, S., and Shevliakova, E.: Climate-vegetation interaction
690 and amplification of Australian dust variability, *Geophys Res Lett*, 43, 11823-
691 11830, 10.1002/2016gl071016, 2016.
- 692 Fecan, F., Marticorena, B., and Bergametti, G.: Parametrization of the increase of the
693 aeolian erosion threshold wind friction velocity due to soil moisture for arid and
694 semi-arid areas, *Ann Geophys-Atm Hydr*, 17, 149-157, DOI
695 10.1007/s005850050744, 1999.
- 696 Fiedler, S., Schepanski, K., Heinold, B., Knippertz, P., and Tegen, I.: Climatology of
697 nocturnal low-level jets over North Africa and implications for modeling mineral
698 dust emission, *J Geophys Res-Atmos*, 118, 6100-6121, 10.1002/jgrd.50394, 2013.
- 699 Fiedler, S., Knippertz, P., Woodward, S., Martin, G. M., Bellouin, N., Ross, A. N.,
700 Heinold, B., Schepanski, K., Birch, C. E., and Tegen, I.: A process-based
701 evaluation of dust-emitting winds in the CMIP5 simulation of HadGEM2-ES,
702 *Clim Dynam*, 46, 1107-1130, 10.1007/s00382-015-2635-9, 2016.



- 703 Fung, I. Y., Meyn, S. K., Tegen, I., Doney, S. C., John, J. G., and Bishop, J. K. B.: Iron
704 supply and demand in the upper ocean, *Global Biogeochem Cy*, 14, 281-295, Doi
705 10.1029/1999gb900059, 2000.
- 706 Fuss, S., Canadell, J. G., Peters, G. P., Tavoni, M., Andrew, R. M., Ciais, P., Jackson, R.
707 B., Jones, C. D., Kraxner, F., Nakicenovic, N., Le Quere, C., Raupach, M. R.,
708 Sharifi, A., Smith, P., and Yamagata, Y.: COMMENTARY: Betting on negative
709 emissions, *Nat Clim Change*, 4, 850-853, DOI 10.1038/nclimate2392, 2014.
- 710 Gillette, D. A., and Passi, R.: Modeling Dust Emission Caused by Wind Erosion, *J*
711 *Geophys Res-Atmos*, 93, 14233-14242, DOI 10.1029/JD093iD11p14233, 1988.
- 712 Ginoux, P., Chin, M., Tegen, I., Prospero, J. M., Holben, B., Dubovik, O., and Lin, S. J.:
713 Sources and distributions of dust aerosols simulated with the GOCART model, *J*
714 *Geophys Res-Atmos*, 106, 20255-20273, Doi 10.1029/2000jd000053, 2001.
- 715 Ginoux, P., Garbuzov, D., and Hsu, N. C.: Identification of anthropogenic and natural
716 dust sources using Moderate Resolution Imaging Spectroradiometer (MODIS)
717 Deep Blue level 2 data, *J Geophys Res-Atmos*, 115, 10.1029/2009jd012398,
718 2010.
- 719 Ginoux, P., Clarisse, L., Clerbaux, C., Coheur, P. F., Dubovik, O., Hsu, N. C., and Van
720 Damme, M.: Mixing of dust and NH₃ observed globally over anthropogenic dust
721 sources, *Atmos Chem Phys*, 12, 7351-7363, 10.5194/acp-12-7351-2012, 2012a.
- 722 Ginoux, P., Prospero, J. M., Gill, T. E., Hsu, N. C., and Zhao, M.: Global-Scale
723 Attribution of Anthropogenic and Natural Dust Sources and Their Emission Rates
724 Based on Modis Deep Blue Aerosol Products, *Rev Geophys*, 50,
725 10.1029/2012rg000388, 2012b.



- 726 Houghton, J., Ding, Y., Griggs, D. J., Noguera, M., Linden, P. J. v. d., Dai, X., Maskell,
727 K., and Johnson, C. A.: Climate Change 2001: The scientific basis. Contribution
728 of Working Group I to the Third Assessment Report of the Intergovernmental
729 Panel on Climate Change, in, Cambridge Univ. Press, Cambridge, UK, 2001.
- 730 Hsu, N. C., Tsay, S. C., King, M. D., and Herman, J. R.: Aerosol properties over bright-
731 reflecting source regions, *Ieee T Geosci Remote*, 42, 557-569,
732 10.1109/Tgrs.2004.824067, 2004.
- 733 Hsu, N. C., Tsay, S. C., King, M. D., and Herman, J. R.: Deep blue retrievals of Asian
734 aerosol properties during ACE-Asia, *Ieee T Geosci Remote*, 44, 3180-3195,
735 10.1109/Tgrs.2006.879540, 2006.
- 736 Huneus, N., Schulz, M., Balkanski, Y., Griesfeller, J., Prospero, J., Kinne, S., Bauer, S.,
737 Boucher, O., Chin, M., Dentener, F., Diehl, T., Easter, R., Fillmore, D., Ghan, S.,
738 Ginoux, P., Grini, A., Horowitz, L., Koch, D., Krol, M. C., Landing, W., Liu, X.,
739 Mahowald, N., Miller, R., Morcrette, J. J., Myhre, G., Penner, J., Perlwitz, J.,
740 Stier, P., Takemura, T., and Zender, C. S.: Global dust model intercomparison in
741 AeroCom phase I, *Atmos Chem Phys*, 11, 7781-7816, 10.5194/acp-11-7781-
742 2011, 2011.
- 743 Jickells, T. D., An, Z. S., Andersen, K. K., Baker, A. R., Bergametti, G., Brooks, N., Cao,
744 J. J., Boyd, P. W., Duce, R. A., Hunter, K. A., Kawahata, H., Kubilay, N.,
745 laRoche, J., Liss, P. S., Mahowald, N., Prospero, J. M., Ridgwell, A. J., Tegen, I.,
746 and Torres, R.: Global iron connections between desert dust, ocean
747 biogeochemistry, and climate, *Science*, 308, 67-71, DOI
748 10.1126/science.1105959, 2005.



- 749 Jin, Q., Wei, J., Yang, Z. L., Pu, B., and Huang, J.: Consistent response of Indian summer
750 monsoon to Middle East dust in observations and simulations, *Atmos Chem Phys*,
751 15, 9897-9915, 10.5194/acp-15-9897-2015, 2015.
- 752 Jin, Q. J., Wei, J. F., and Yang, Z. L.: Positive response of Indian summer rainfall to
753 Middle East dust, *Geophys Res Lett*, 41, 4068-4074, 10.1002/2014gl059980,
754 2014.
- 755 Jin, Q. J., Yang, Z. L., and Wei, J. F.: Seasonal Responses of Indian Summer Monsoon to
756 Dust Aerosols in the Middle East, India, and China, *J Climate*, 29, 6329-6349,
757 10.1175/Jcli-D-15-0622.1, 2016.
- 758 Kim, M. K., Lau, W. K. M., Kim, K. M., Sang, J., Kim, Y. H., and Lee, W. S.:
759 Amplification of ENSO effects on Indian summer monsoon by absorbing
760 aerosols, *Clim Dynam*, 46, 2657-2671, 10.1007/s00382-015-2722-y, 2016.
- 761 Kok, J. F., Ridley, D. A., Zhou, Q., Miller, R. L., Zhao, C., Heald, C. L., Ward, D. S.,
762 Albani, S., and Haustein, K.: Smaller desert dust cooling effect estimated from
763 analysis of dust size and abundance, *Nat Geosci*, 10, 274-+, 10.1038/Ngeo2912,
764 2017.
- 765 Laurent, B., Marticorena, B., Bergametti, G., and Mei, F.: Modeling mineral dust
766 emissions from Chinese and Mongolian deserts, *Global Planet Change*, 52, 121-
767 141, 10.1016/j.gloplacha.2006.02.012, 2006.
- 768 Levin, Z., Ganor, E., and Gladstein, V.: The effects of desert particles coated with sulfate
769 on rain formation in the eastern Mediterranean, *J Appl Meteorol*, 35, 1511-1523,
770 Doi 10.1175/1520-0450(1996)035<1511:Teodpc>2.0.Co;2, 1996.



- 771 Levy, R. C., Mattoo, S., Munchak, L. A., Remer, L. A., Sayer, A. M., Patadia, F., and
772 Hsu, N. C.: The Collection 6 MODIS aerosol products over land and ocean,
773 Atmos Meas Tech, 6, 2989-3034, 10.5194/amt-6-2989-2013, 2013.
- 774 Mahowald, N. M., and Luo, C.: A less dusty future?, Geophys Res Lett, 30,
775 10.1029/2003gl017880, 2003.
- 776 Mahowald, N. M., Kloster, S., Engelstaedter, S., Moore, J. K., Mukhopadhyay, S.,
777 McConnell, J. R., Albani, S., Doney, S. C., Bhattacharya, A., Curran, M. A. J.,
778 Flanner, M. G., Hoffman, F. M., Lawrence, D. M., Lindsay, K., Mayewski, P. A.,
779 Neff, J., Rothenberg, D., Thomas, E., Thornton, P. E., and Zender, C. S.:
780 Observed 20th century desert dust variability: impact on climate and
781 biogeochemistry, Atmos Chem Phys, 10, 10875-10893, 10.5194/acp-10-10875-
782 2010, 2010.
- 783 Marticorena, B., and Bergametti, G.: Modeling the Atmospheric Dust Cycle .1. Design of
784 a Soil-Derived Dust Emission Scheme, J Geophys Res-Atmos, 100, 16415-16430,
785 Doi 10.1029/95jd00690, 1995.
- 786 Marx, S. K., McGowan, H. A., and Kamber, B. S.: Long-range dust transport from
787 eastern Australia: A proxy for Holocene aridity and ENSO-type climate
788 variability, Earth Planet Sc Lett, 282, 167-177, 10.1016/j.epsl.2009.03.013, 2009.
- 789 McConnell, J. R., Aristarain, A. J., Banta, J. R., Edwards, P. R., and Simoes, J. C.: 20th-
790 Century doubling in dust archived in an Antarctic Peninsula ice core parallels
791 climate change and desertification in South America, P Natl Acad Sci USA, 104,
792 5743-5748, 10.1073/pnas.0607657104, 2007.



- 793 Miller, R. L., and Tegen, I.: Climate response to soil dust aerosols, *J Climate*, 11, 3247-
794 3267, Doi 10.1175/1520-0442(1998)011<3247:Crtsda>2.0.Co;2, 1998.
- 795 Miller, R. L., Tegen, I., and Perlwitz, J.: Surface radiative forcing by soil dust aerosols
796 and the hydrologic cycle, *J Geophys Res-Atmos*, 109, 10.1029/2003jd004085,
797 2004.
- 798 Misra, A., Kanawade, V. P., and Tripathi, S. N.: Quantitative assessment of AOD from
799 17 CMIP5 models based on satellite-derived AOD over India, *Ann Geophys-*
800 *Germany*, 34, 657-671, 10.5194/angeo-34-657-2016, 2016.
- 801 Moulin, C., and Chiapello, I.: Impact of human-induced desertification on the
802 intensification of Sahel dust emission and export over the last decades, *Geophys*
803 *Res Lett*, 33, 10.1029/2006gl025923, 2006.
- 804 Myhre, G., Shindell, D., Bréon, F.-M., Collins, W., Fuglestedt, J., Huang, J., Koch, D.,
805 Lamarque, J.-F., Lee, D., Mendoza, B., Nakajima, T., Robock, A., Stephens, G.,
806 Takemura, T., and Zhang, H.: Anthropogenic and Natural Radiative Forcing. , in:
807 *Climate Change 2013: The Physical Science Basis. Contribution of Working*
808 *Group I to the Fifth Assessment Report of the Intergovernmental Panel on*
809 *Climate Change*, edited by: Stocker, T. F., Qin, D., Plattner, G.-K., Tignor, M.,
810 Allen, S. K., Boschung, J., Nauels, A., Xia, Y., Bex, V., and Midgley, P. M.,
811 Cambridge University Press, Cambridge, United Kingdom and New York, NY,
812 USA, 2013.
- 813 Nakajima, T., Higurashi, A., Kawamoto, K., and Penner, J. E.: A possible correlation
814 between satellite-derived cloud and aerosol microphysical parameters, *Geophys*
815 *Res Lett*, 28, 1171-1174, Doi 10.1029/2000gl012186, 2001.



- 816 Neff, J. C., Reynolds, R. L., Belnap, J., and Lamothe, P.: Multi-decadal impacts of
817 grazing on soil physical and biogeochemical properties in southeast Utah, *Ecol*
818 *Appl*, 15, 87-95, Doi 10.1890/04-0268, 2005.
- 819 Neff, J. C., Ballantyne, A. P., Farmer, G. L., Mahowald, N. M., Conroy, J. L., Landry, C.
820 C., Overpeck, J. T., Painter, T. H., Lawrence, C. R., and Reynolds, R. L.:
821 Increasing eolian dust deposition in the western United States linked to human
822 activity, *Nat Geosci*, 1, 189-195, 10.1038/ngeo133, 2008.
- 823 O'Brien, R. M.: A caution regarding rules of thumb for variance inflation factors, *Qual*
824 *Quant*, 41, 673-690, 10.1007/s11135-006-9018-6, 2007.
- 825 O'Neill, N. T., Eck, T. F., Smirnov, A., Holben, B. N., and Thulasiraman, S.: Spectral
826 discrimination of coarse and fine mode optical depth, *J Geophys Res-Atmos*, 108,
827 10.1029/2002jd002975, 2003.
- 828 Prospero, J. M., and Nees, R. T.: Impact of the North African Drought and El-Nino on
829 Mineral Dust in the Barbados Trade Winds, *Nature*, 320, 735-738, DOI
830 10.1038/320735a0, 1986.
- 831 Prospero, J. M., and Lamb, P. J.: African droughts and dust transport to the Caribbean:
832 Climate change implications, *Science*, 302, 1024-1027, DOI
833 10.1126/science.1089915, 2003.
- 834 Pu, B., Fu, R., Dickinson, R. E., and Fernando, D. N.: Why do summer droughts in the
835 Southern Great Plains occur in some La Nina years but not others?, *J Geophys*
836 *Res-Atmos*, 121, 1120-1137, 10.1002/2015jd023508, 2016.



- 837 Pu, B., and Ginoux, P.: The impact of the Pacific Decadal Oscillation on springtime dust
838 activity in Syria, *Atmos Chem Phys*, 16, 13431-13448, 10.5194/acp-16-13431-
839 2016, 2016.
- 840 Pu, B., and Ginoux, P.: Projection of American dustiness in the late 21st century due to
841 climate change, *Scientific reports*, 7, 10.1038/s41598-017-05431-9, 2017.
- 842 Reader, M. C., Fung, I., and McFarlane, N.: The mineral dust aerosol cycle during the
843 last glacial maximum (vol 104, pg 9381, 1999), *J Geophys Res-Atmos*, 104,
844 22319-22320, Doi 10.1029/1999jd900434, 1999.
- 845 Riahi, K., Rao, S., Krey, V., Cho, C. H., Chirkov, V., Fischer, G., Kindermann, G.,
846 Nakicenovic, N., and Rafaj, P.: RCP 8.5-A scenario of comparatively high
847 greenhouse gas emissions, *Climatic Change*, 109, 33-57, 10.1007/s10584-011-
848 0149-y, 2011.
- 849 Rosenfield, J. E., Considine, D. B., Meade, P. E., Bacmeister, J. T., Jackman, C. H., and
850 Schoeberl, M. R.: Stratospheric effects of Mount Pinatubo aerosol studied with a
851 coupled two-dimensional model, *J Geophys Res-Atmos*, 102, 3649-3670, Doi
852 10.1029/96jd03820, 1997.
- 853 Sanap, S. D., Ayantika, D. C., Pandithurai, G., and Niranjana, K.: Assessment of the
854 aerosol distribution over Indian subcontinent in CMIP5 models, *Atmospheric
855 Environment*, 87, 123-137, 10.1016/j.atmosenv.2014.01.017, 2014.
- 856 Seland, O., Iversen, T., Kirkevåg, A., and Storelvmo, T.: Aerosol-climate interactions in
857 the CAM-Oslo atmospheric GCM and investigation of associated basic
858 shortcomings, *Tellus A*, 60, 459-491, 10.1111/j.1600-0870.2008.00318.x, 2008.



- 859 Shao, Y. P., Wyrwoll, K. H., Chappell, A., Huang, J. P., Lin, Z. H., McTainsh, G. H.,
860 Mikami, M., Tanaka, T. Y., Wang, X. L., and Yoon, S.: Dust cycle: An emerging
861 core theme in Earth system science, *Aeolian Res*, 2, 181-204,
862 10.1016/j.aeolia.2011.02.001, 2011.
- 863 Sharma, D., and Miller, R. L.: Revisiting the observed correlation between weekly
864 averaged Indian monsoon precipitation and Arabian Sea aerosol optical depth,
865 *Geophys Res Lett*, 44, 10006-10016, 10.1002/2017gl074373, 2017.
- 866 Shindell, D. T., Lamarque, J. F., Schulz, M., Flanner, M., Jiao, C., Chin, M., Young, P. J.,
867 Lee, Y. H., Rotstajn, L., Mahowald, N., Milly, G., Faluvegi, G., Balkanski, Y.,
868 Collins, W. J., Conley, A. J., Dalsoren, S., Easter, R., Ghan, S., Horowitz, L., Liu,
869 X., Myhre, G., Nagashima, T., Naik, V., Rumbold, S. T., Skeie, R., Sudo, K.,
870 Szopa, S., Takemura, T., Voulgarakis, A., Yoon, J. H., and Lo, F.: Radiative
871 forcing in the ACCMIP historical and future climate simulations, *Atmos Chem*
872 *Phys*, 13, 2939-2974, 10.5194/acp-13-2939-2013, 2013.
- 873 Solmon, F., Nair, V. S., and Mallet, M.: Increasing Arabian dust activity and the Indian
874 summer monsoon, *Atmos Chem Phys*, 15, 8051-8064, 10.5194/acp-15-8051-
875 2015, 2015.
- 876 Strong, J. D., Vecchi, G. A., and Ginoux, P.: The Climatological Effect of Saharan Dust
877 on Global Tropical Cyclones in a Fully Coupled GCM, *Journal of Geophysical*
878 *Research - Atmospheres* (under review), 2018.
- 879 Strong, J. D. O., Vecchi, G. A., and Ginoux, P.: The Response of the Tropical Atlantic
880 and West African Climate to Saharan Dust in a Fully Coupled GCM, *J Climate*,
881 28, 7071-7092, 10.1175/Jcli-D-14-00797.1, 2015.



- 882 Sun, D. L., Lau, K. M., and Kafatos, M.: Contrasting the 2007 and 2005 hurricane
883 seasons: Evidence of possible impacts of Saharan dry air and dust on tropical
884 cyclone activity in the Atlantic basin, *Geophys Res Lett*, 35,
885 10.1029/2008gl034529, 2008.
- 886 Takemura, T., Okamoto, H., Maruyama, Y., Numaguti, A., Higurashi, A., and Nakajima,
887 T.: Global three-dimensional simulation of aerosol optical thickness distribution
888 of various origins, *J Geophys Res-Atmos*, 105, 17853-17873, Doi
889 10.1029/2000jd900265, 2000.
- 890 Tegen, I., Harrison, S. P., Kohfeld, K., Prentice, I. C., Coe, M., and Heimann, M.: Impact
891 of vegetation and preferential source areas on global dust aerosol: Results from a
892 model study, *J Geophys Res-Atmos*, 107, 10.1029/2001jd000963, 2002.
- 893 Tegen, I., Werner, M., Harrison, S. P., and Kohfeld, K. E.: Relative importance of
894 climate and land use in determining present and future global soil dust emission,
895 *Geophys Res Lett*, 31, 10.1029/2003gl019216, 2004.
- 896 Todd, M. C., Washington, R., Raghavan, S., Lizcano, G., and Knippertz, P.: Regional
897 model simulations of the Bodele low-level jet of northern Chad during the Bodele
898 Dust Experiment (BoDEx 2005), *J Climate*, 21, 995-1012,
899 10.1175/2007jcli1766.1, 2008.
- 900 Vinoj, V., Rasch, P. J., Wang, H. L., Yoon, J. H., Ma, P. L., Landu, K., and Singh, B.:
901 Short-term modulation of Indian summer monsoon rainfall by West Asian dust,
902 *Nat Geosci*, 7, 308-313, 10.1038/ngeo2107, 2014.
- 903 Watanabe, S., Hajima, T., Sudo, K., Nagashima, T., Takemura, T., Okajima, H., Nozawa,
904 T., Kawase, H., Abe, M., Yokohata, T., Ise, T., Sato, H., Kato, E., Takata, K.,



- 905 Emori, S., and Kawamiya, M.: MIROC-ESM 2010: model description and basic
906 results of CMIP5-20c3m experiments, *Geosci Model Dev*, 4, 845-872,
907 10.5194/gmd-4-845-2011, 2011.
- 908 Winker, D. M., Hunt, W., and Hostetler, C.: Status and performance of the CALIOP
909 lidar, *Bba Lib*, 5575, 8-15, 10.1117/12.571955, 2004.
- 910 Winker, D. M., Hunt, W. H., and McGill, M. J.: Initial performance assessment of
911 CALIOP, *Geophys Res Lett*, 34, 10.1029/2007gl030135, 2007.
- 912 Wong, S., and Dessler, A. E.: Suppression of deep convection over the tropical North
913 Atlantic by the Saharan Air Layer, *Geophys Res Lett*, 32, 10.1029/2004gl022295,
914 2005.
- 915 Wurzler, S., Reisin, T. G., and Levin, Z.: Modification of mineral dust particles by cloud
916 processing and subsequent effects on drop size distributions, *J Geophys Res-*
917 *Atmos*, 105, 4501-4512, Doi 10.1029/1999jd900980, 2000.
- 918 Zender, C. S., and Kwon, E. Y.: Regional contrasts in dust emission responses to climate,
919 *J Geophys Res-Atmos*, 110, 10.1029/2004jd005501, 2005.
- 920 Zhao, T. L., Gong, S. L., Zhang, X. Y., Blanchet, J. P., McKendry, I. G., and Zhou, Z. J.:
921 A simulated climatology of Asian dust aerosol and its trans-Pacific transport. Part
922 I: Mean climate and validation, *J Climate*, 19, 88-103, Doi 10.1175/Jcli3605.1,
923 2006.
- 924
- 925
- 926



927 Table 1 CMIP5 models used in this study. Models tagged with plus signs (+) considered
928 anthropogenic land use/land cover change in their vegetation prediction.

929

930 Table 2 List of regions selected to compare model output with MODIS DOD. Locations
931 of these regions are also plotted in Fig. 1b. Acronyms are used for some regions for short,
932 and are listed in the brackets in the first column. Note that the region names such as
933 Northern China and India are not exactly the same as their geographical definitions but
934 also covers some areas from nearby countries.

935

936 Table 3 Changes of DOD in the late half of the 21st century (2051-2100; RCP 8.5
937 scenario) from the historical condition (1861-2005) projected by CMIP5 multi-model
938 mean (second to fifth columns) and the regression model (sixth to ninth columns) in the
939 nine regions. Changes of DOD are shown in percentage with reference to CMIP5 multi-
940 model historical run. Note that in some regions the projected change by the regression
941 model is quite large (i.e., greater than $\pm 100\%$), largely due to the underestimation of
942 CMIP5 historical run in these regions.

943

944

945

946

947

948

949



950 Figure 1. Figure 1. Climatology (2004-2016) of Aqua and Terra combined DOD (i.e.,
951 MODIS DOD; top panel) and multi-model mean of CMIP5 DOD (bottom) for four
952 seasons. The pattern correlation (centered; calculated after interpolating MODIS DOD to
953 CMIP5 DOD grids) between CMIP5 and MODIS DOD are shown in pink in the bottom
954 panel. Blue numbers denote global mean DOD over land. For CMIP5 model results, \pm
955 one standard deviation among seven CMIP5 models is also shown. Black boxes in (b)
956 denote nine averaging regions (Table 2). Here we only added these boxes in (b) instead of
957 every plot to keep the figure clean. Note that CMIP5 multi-model mean is masked by
958 MODIS DOD for comparison. Dotted area in (e)-(h) shows where multi-model mean is
959 greater than one inter-model standard deviation.

960

961 Figure 2. Zonal mean DOD from MODIS (thick red), CMIP5 multi-model mean (thick
962 black), and each individual model (other colorful lines).

963

964 Figure 3. Seasonal cycle of DOD in nine regions (Table 2) averaged over 2004-2016.
965 Thick red lines denote MODIS DOD, thick black lines denote CMIP5 multi-model mean,
966 and other colorful lines denote individual model output. The annual means from MODIS
967 DOD (Obs; red) and multi-model mean (Ens; black) are shown in each panel.

968

969 Figure 4. Spatial statistics comparing DOD from CMIP5 models with that from MODIS
970 in nine regions. Label on the X-axis shows individual models (1-7) and multi-model
971 mean (8). Y-axis shows the ratio of pattern standard deviations between model
972 climatology (2004-2016) and that of MODIS, which reveals the relative amplitude of the



973 simulated DOD versus satellite DOD. The color denotes pattern correlation (centered)
974 between each model and MODIS DOD in each region.

975

976 Figure 5. Correlations (color) between regional averaged time series from CMIP5 DOD
977 and MODIS DOD from 2004 to 2016 for four seasons. Numbers in the X-axis denotes
978 each model (1-7) and multi-model mean (8). Correlations significant at the 90%
979 confidence level are marked by a star and significance at the 95% confidence level by
980 two stars.

981

982 Figure 6. Regression coefficients calculated by regressing DOD in each season onto
983 standardized precipitation (purple), bareness (orange), and surface wind speed (green)
984 from 2004 to 2016. Coefficients obtained using MODIS DOD and observed controlling
985 factors and those using CMIP5 multi-model mean DOD and controlling factors are
986 shown in the left and right columns, respectively. The color of the shading denotes the
987 largest coefficient in absolute value among the three, while the saturation of the color
988 shows the magnitude of the coefficient (from 0 to 0.02). Only regression coefficients
989 significant at the 90% confidence level (Bootstrap test) are shown. Missing values are
990 shaded in grey. To highlight coefficients near the source regions, a mask of $LAI \leq 0.5$ is
991 applied.

992

993 Figure 7. Projected changes of DOD in the late half of the 21st century (under the RCP
994 8.5 scenario) from that in the historical level (1861-2005) by CMIP5 multi-model mean
995 for four seasons. The percentage change of global mean (over land) DOD \pm one inter-



996 among the models reaches 71.4% (i.e., at least five out seven models have the same sign
997 as the multi-model mean) are dotted.

998

999 Figure 8. Projected difference of (a)-(d) precipitation (mm day⁻¹), (e)-(h) bareness, and
1000 (i)-(l) 10 m wind (m s⁻¹) between the late half of the 21st century (2051-2100; RCP 8.5
1001 scenario) and historical level (1861-2005) from multi-model mean of seven CMIP5
1002 models. Areas with sign agreement among the models reaches 71.4% (i.e., at least five
1003 out seven models have the same sign as the multi-model mean) are dotted.

1004

1005 Figure 9. Projected change of DOD in the late half of the 21st century under the RCP 8.5
1006 scenario by the regression model. The results are calculated using the regression
1007 coefficients obtained from observations during 2004-2016 (see methodology) and
1008 projected changes of precipitation, bareness, and surface wind from 16 CMIP5 models.
1009 Dotted areas are regions with sign agreement among the models above 62.5% (i.e., at
1010 least 10 out 16 models have the same sign as the multi-model mean). To highlight DOD
1011 variations near the source regions, a mask of LAI ≤ 0.5 (from present-day climatology) is
1012 applied.

1013

1014 Figure 10. (a)-(d) Projected change of DOD in the late half of the 21st century under the
1015 RCP 8.5 scenario by the regression model (same as Fig. 9), and contributions from each
1016 component, (e)-(h) precipitation, (j)-(i) bareness, and (m)-(p) surface wind speed. Dotted
1017 areas are regions with sign agreement among the models above 62.5%. To highlight



1018 DOD variations near the source regions, a mask of $LAI \leq 0.5$ (from present-day
1019 climatology) is applied.

1020

1021

1022

1023

1024

1025

1026

1027

1028

1029

1030

1031

1032

1033

1034

1035

1036

1037

1038

1039

1040



1041

1042 Table 1 CMIP5 models used in this study. Models tagged with plus signs (+) considered

1043 anthropogenic land use/land cover change in their vegetation prediction.

1044

Model	lat/lon resolution	Dust emission scheme	Dynamic Vegetation	Model reference
CanESM2	2.8°×2.8°	Reader et al. (1999); Croft et al. (2005)	N ⁺	Arora et al. (2011)
GFDL-CM3	2.0°×2.5°	Ginoux et al. (2001)	Y ⁺	Donner et al. (2011)
HadGEM2-CC	1.2°×1.8°	Marticorena and Bergametti (1995)	Y ⁺	Collins et al. (2011)
HadGEM2-ES	1.2°×1.8°	Marticorena and Bergametti (1995)	Y ⁺	Collins et al. (2011)
MIROC-ESM	2.8°×2.8°	Takemura et al. (2000)	Y ⁺	Watanabe et al. (2011)
MIROC-ESM-CHEM	2.8°×2.8°	Takemura et al. (2000)	Y ⁺	Watanabe et al. (2011)
NorESM1-M	1.9°×2.5°	Seland et al. (2008)	N ⁺	Bentsen et al. (2013)

1045

1046

1047

1048

1049

1050

1051

1052

1053

1054

1055

1056

1057

1058

1059

1060

1061

1062

1063

1064

1065

1066

1067

1068

1069

1070

1071

1072

1073

1074

1075
1076
1077
1078
1079
1080
1081

Table 2 List of regions selected to compare model output with MODIS DOD. Locations of these regions are also plotted in Fig. 1b. Acronyms are used for some regions for short, and are listed in the brackets in the first column. Note that the region names such as Northern China and India are not exactly the same as their geographical definitions but also covers some areas from nearby countries.

Region	Domain
North Africa (N. Africa)	5°-50°N, 18°W-35°E
Middle East	12°-50°N, 35°-60°E
Northern China (N. China)	35°-50°N, 70°-110°E
North America (N. America)	25°-50°N, 95°-125°W
India	5°-35°N, 60°-90°E
Southeastern Asia (SE. Asia)	9°-35°N, 90°-121°E
South Africa (S. Africa)	15°-35°S, 10°-50°E
South America (S. America)	0°-55°S, 60°-83°W
Australia	10°-40°S, 112°-155°E

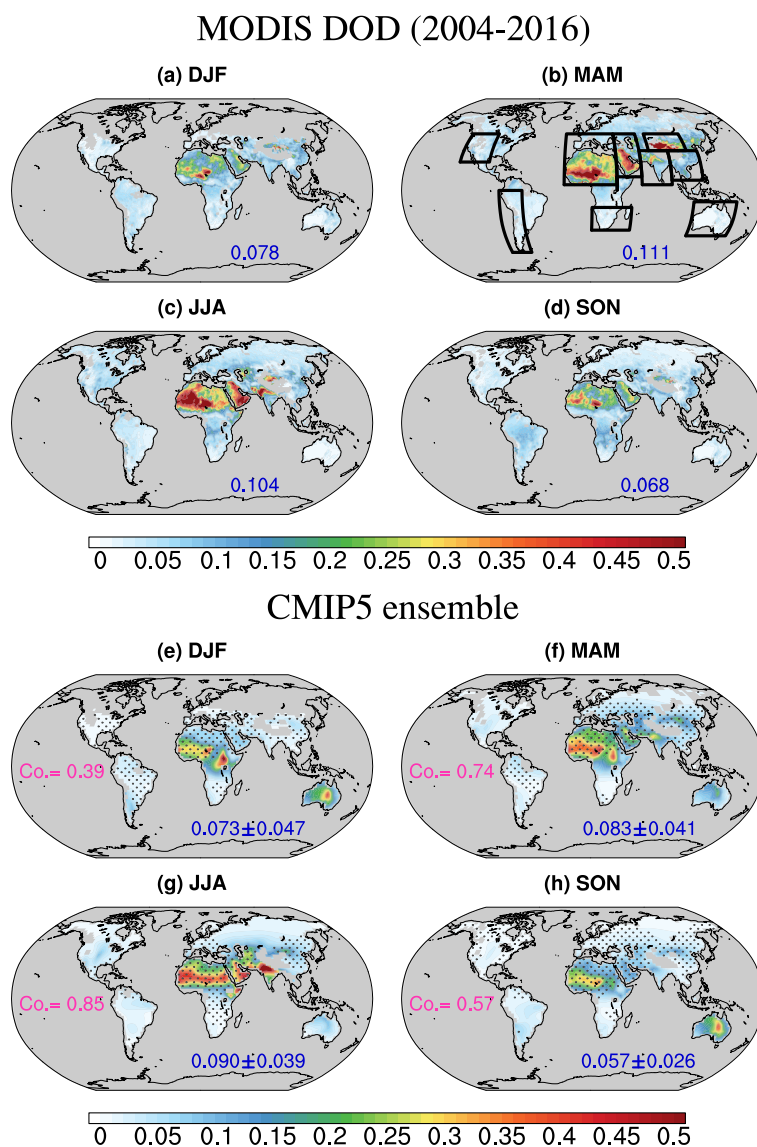
1082
1083
1084
1085
1086
1087
1088
1089
1090
1091
1092
1093
1094
1095
1096
1097
1098
1099
1100
1101
1102
1103
1104
1105
1106
1107
1108
1109
1110

1111
1112
1113
1114
1115
1116
1117
1118
1119

Table 3 Changes of DOD in the late half of the 21st century (2051-2100; RCP 8.5 scenario) from the historical condition (1861-2005) projected by CMIP5 multi-model mean (second to fifth columns) and the regression model (sixth to ninth columns) in nine regions. Changes of DOD are shown in percentage with reference to CMIP5 multi-model historical run. Note that in some regions the projected change by the regression model is quite large (i.e., greater than $\pm 100\%$), largely due to the underestimation of CMIP5 historical run in these regions.

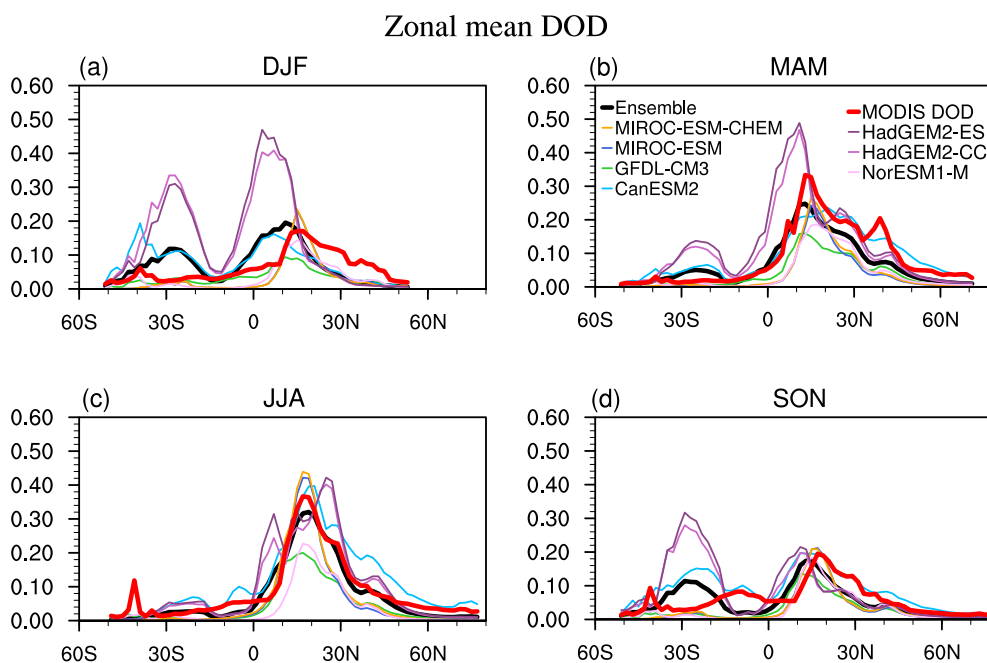
Region	CMIP5				Regression model			
	DJF	MAM	JJA	SON	DJF	MAM	JJA	SON
N. Africa	-3.8	-3.6	2.4	-16.3	-0.8	-17.7	11.1	-10.3
Middle East	7.8	4.5	6.4	1.5	9.8	-16.0	-5.4	-8.4
N. China	-33.5	-11.4	-9.8	-14.4	312.3	-238.6	-51.2	-30.0
N. America	42.6	26.8	13.2	-6.4	-38.5	-90.0	9.3	-42.4
India	-5.1	0.2	-1.0	-9.9	-27.6	-8.2	-2.9	-32.3
SE. Asia	-45.7	-16.5	-13.5	-17.1	-34.8	1.6	4.2	96.3
S. Africa	24.0	6.1	38.5	54.4	22.3	59.3	231.8	78.3
S. America	35.7	27.4	51.8	36.0	14.8	56.1	78.3	154.6
Australia	-3.2	-3.2	15.3	17.0	2.7	0.4	0.7	3.7

1120
1121
1122
1123
1124



1125
 1126
 1127
 1128
 1129
 1130
 1131
 1132
 1133
 1134
 1135

Figure 1. Climatology (2004-2016) of Aqua and Terra combined DOD (i.e., MODIS DOD; top panel) and multi-model mean of CMIP5 DOD (bottom) for four seasons. The pattern correlation (centered; calculated after interpolating MODIS DOD to CMIP5 DOD grids) between CMIP5 and MODIS DOD are shown in pink in the bottom panel. Blue numbers denote global mean DOD over land. For CMIP5 model results, \pm one standard deviation among seven CMIP5 models is also shown. Black boxes in (b) denote nine averaging regions (Table 2). Here we only added these boxes in (b) instead of every plot to keep the figure clean. Note that CMIP5 multi-model mean is masked by MODIS DOD for comparison. Dotted area in (e)-(h) shows where multi-model mean is greater than one inter-model standard deviation.



1136

1137 Figure 2. Zonal mean DOD from MODIS (thick red), CMIP5 multi-model mean (thick

1138 black), and each individual model (other colorful lines).

1139

1140

1141

1142

1143

1144

1145

1146

1147

1148

1149

1150

1151

1152

1153

1154

1155

1156

1157

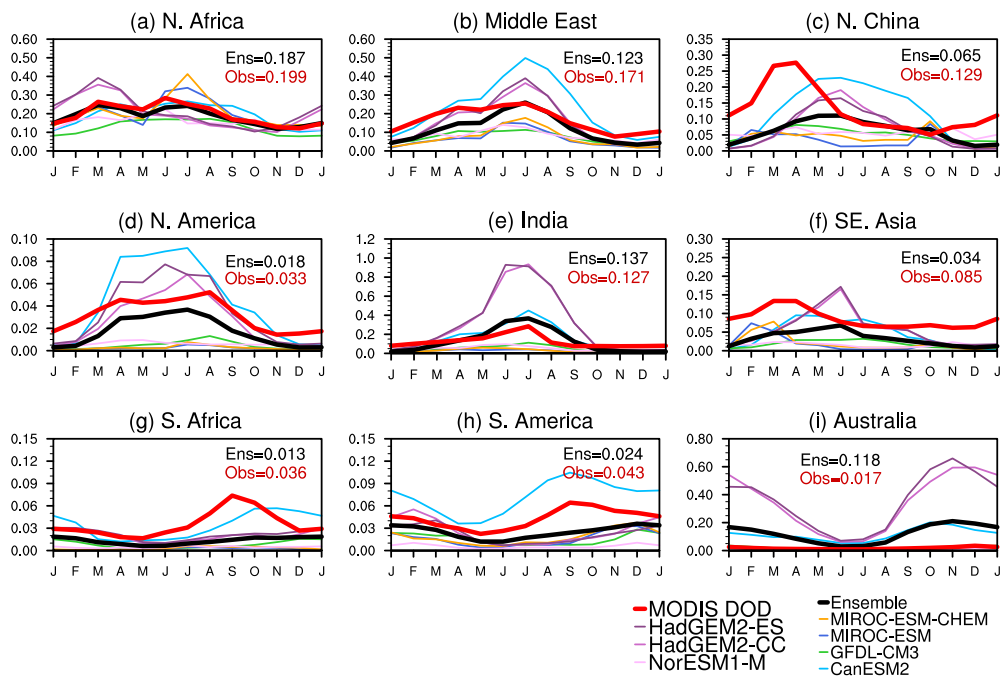
1158

1159

1160



Dust optical depth (2004-2016)



1161

1162

Figure 3. Seasonal cycle of DOD in nine regions (Table 2) averaged over 2004-2016.

1163

Thick red lines denote MODIS DOD, thick black lines denote CMIP5 multi-model mean,

1164

and other colorful lines denote individual model output. The annual means from MODIS

1165

DOD (Obs; red) and multi-model mean (Ens; black) are also listed in each panel.

1166

1167

1168

1169

1170

1171

1172

1173

1174

1175

1176

1177

1178

1179

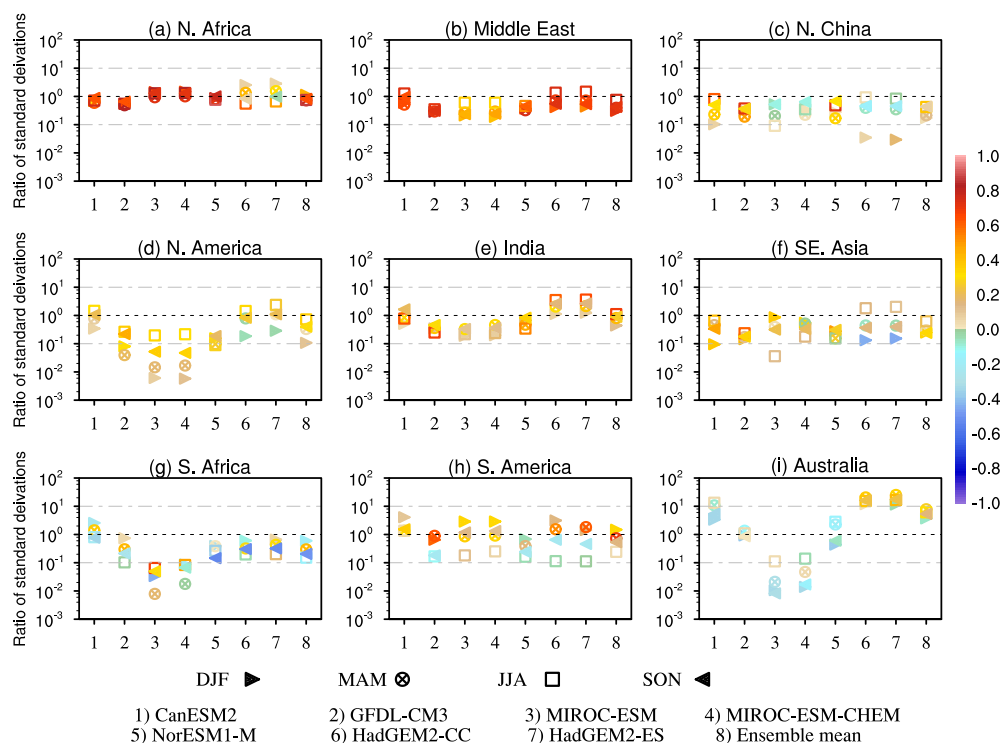
1180

1181

1182

1183

1184



1185

1186

1187 Figure 4. Spatial statistics comparing DOD from CMIP5 models with that from MODIS

1188 in nine regions. Label on the X-axis shows individual models (1-7) and multi-model

1189 mean (8). Y-axis shows the ratio of pattern standard deviations between model

1190 climatology (2004-2016) and that of MODIS, which reveals the relative amplitude of the

1191 simulated DOD versus satellite DOD. The color denotes pattern correlation (centered)

1192 between each model and MODIS DOD in each region.

1193

1194

1195

1196

1197

1198

1199

1200

1201

1202

1203

1204

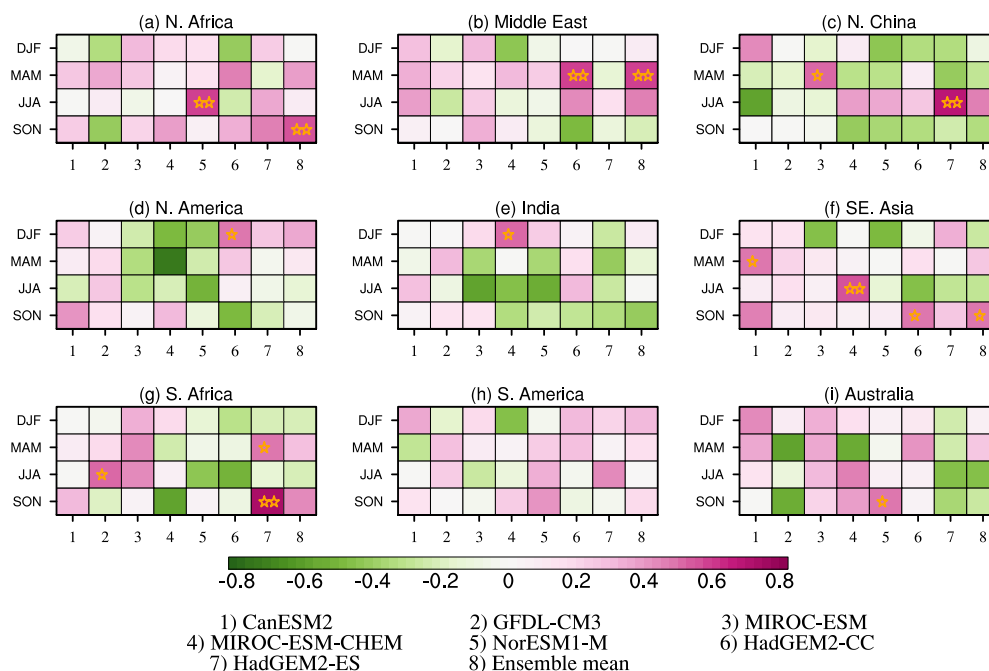
1205

1206

1207



DOD (CMIP5 vs. MODIS)



1208

1209

1210

1211

1212

1213

1214

1215

1216

1217

1218

1219

1220

1221

1222

1223

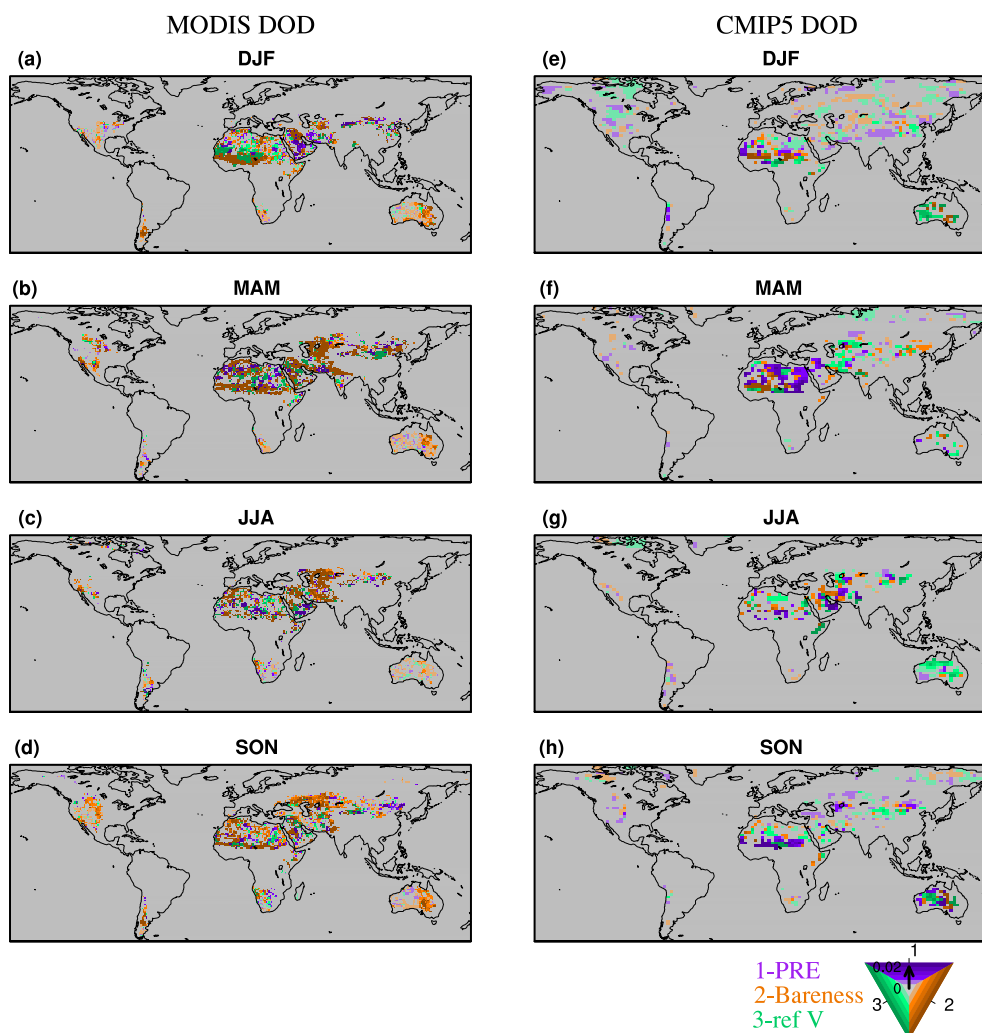
1224

1225

1226

1227

Figure 5. Correlations (color) between regional averaged time series from CMIP5 DOD and MODIS DOD from 2004 to 2016 for four seasons. Numbers in the X-axis denotes each model (1-7) and multi-model mean (8). Correlations significant at the 90% confidence level are marked by a star and significance at the 95% confidence level by two stars.



1228

1229

1230 Figure 6. Regression coefficients calculated by regressing DOD in each season onto

1231 standardized precipitation (purple), bareness (orange), and surface wind speed (green)

1232 from 2004 to 2016. Coefficients obtained using MODIS DOD and observed controlling

1233 factors and those using CMIP5 multi-model mean DOD and controlling factors are

1234 shown in the left and right columns, respectively. The color of the shading denotes the

1235 largest coefficient in absolute value among the three, while the saturation of the color

1236 shows the magnitude of the coefficient (from 0 to 0.02). Only regression coefficients

1237 significant at the 90% confidence level (Bootstrap test) are shown. Missing values are

1238 shaded in grey. To highlight coefficients near dust source regions, a mask of $LAI \leq 0.5$

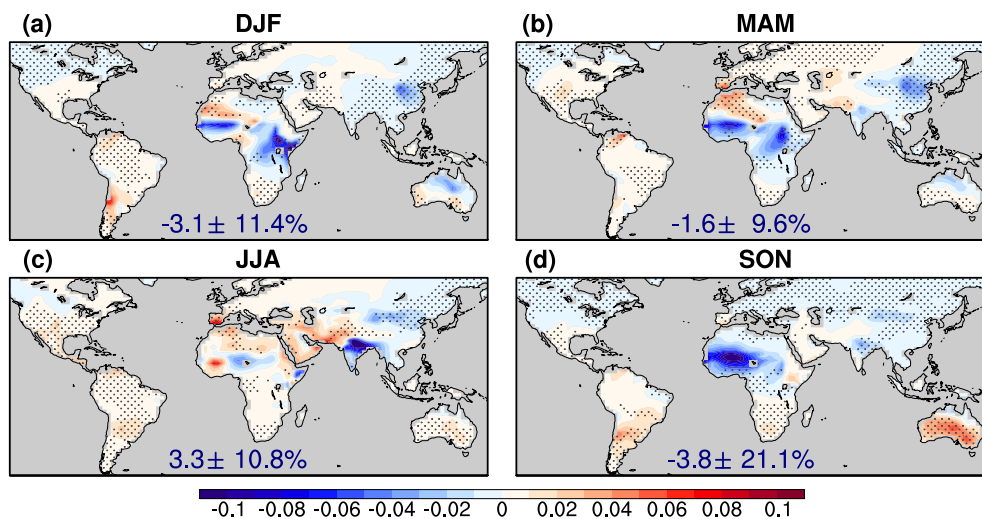
1239 is applied.

1240

1241



Changes of CMIP5 DOD (2051-2100 minus 1861-2005)



1242

1243

1244 Figure 7. Projected changes of DOD in the late half of the 21st century (under the RCP

1245 8.5 scenario) from that in the historical level (1861-2005) by CMIP5 multi-model mean

1246 for four seasons. The percentage change of global mean (over land) DOD ± one inter-

1247 model standard deviation is shown at the bottom of each plot. Areas with sign agreement

1248 among the models reaches 71.4% (i.e., at least five out seven models have the same sign

1249 as the multi-model mean) are dotted.

1249

1250

1251

1252

1253

1254

1255

1256

1257

1258

1259

1260

1261

1262

1263

1264

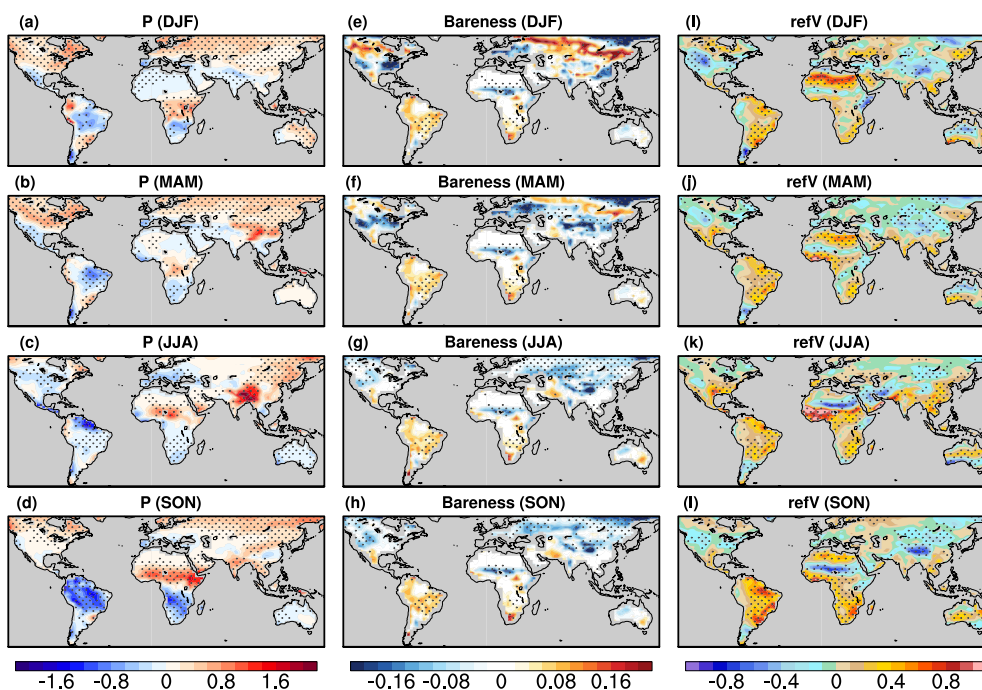
1265

1266

1267

1268

1269



1270

1271 Figure 8. Projected difference of (a)-(d) precipitation (mm day^{-1}), (e)-(h) bareness, and

1272 (i)-(l) 10 m wind (m s^{-1}) between the late half of the 21st century (2051-2100; RCP 8.5

1273 scenario) and historical level (1861-2005) from multi-model mean of seven CMIP5

1274 models. Areas with sign agreement among the models reaches 71.4% (i.e., at least five

1275 out seven models have the same sign as the multi-model mean) are dotted.

1276

1277

1278

1279

1280

1281

1282

1283

1284

1285

1286

1287

1288

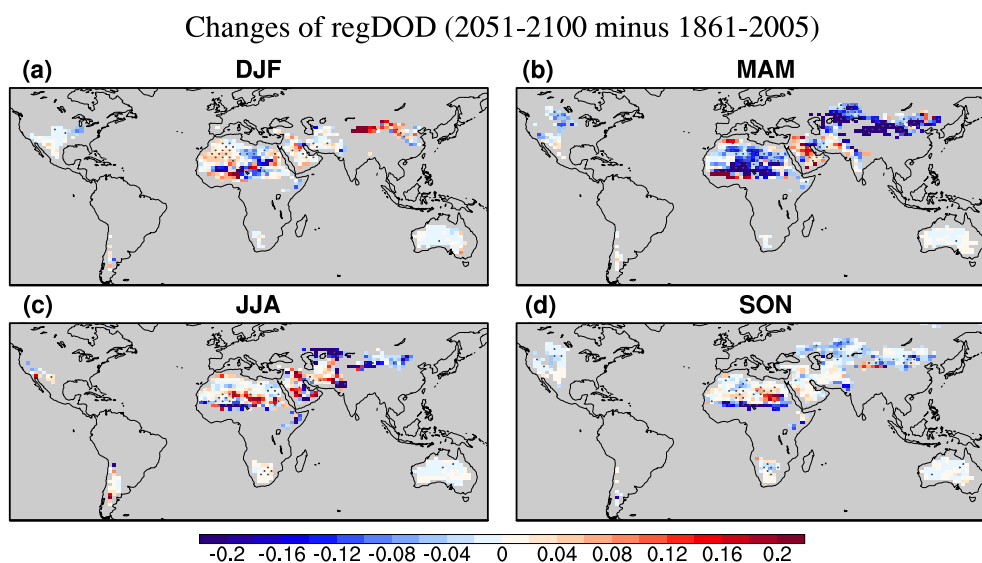
1289

1290

1291

1292

1293



1294

1295

1296 Figure 9. Projected change of DOD in the late half of the 21st century under the RCP 8.5

1297 scenario by the regression model. The results are calculated using the regression

1298 coefficients obtained from observations during 2004-2016 (see methodology) and

1299 projected changes of precipitation, bareness, and surface wind from 16 CMIP5 models.

1300 Dotted areas are regions with sign agreement among the models above 62.5% (i.e., at

1301 least 10 out of 16 models have the same sign as the multi-model mean). To highlight DOD

1302 variations near the source regions, a mask of LAI ≤ 0.5 (from present-day climatology) is

1303 applied.

1304

1305

1306

1307

1308

1309

1310

1311

1312

1313

1314

1315

1316

1317

1318

1319

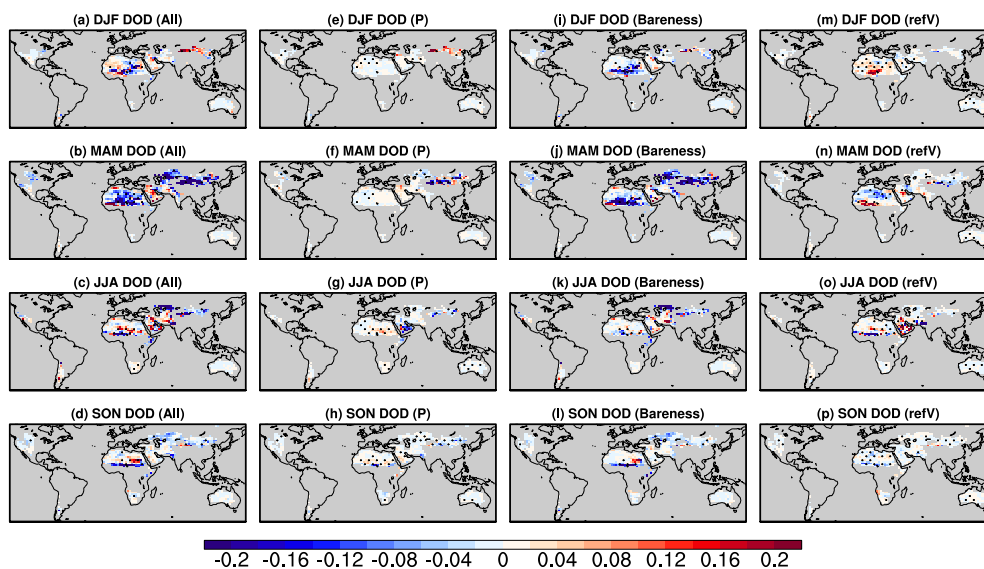
1320

1321

1322



Changes of DOD (2051-2100 minus 1861-2005)



1323
1324
1325
1326
1327
1328
1329
1330

Figure 10. (a)-(d) Projected change of DOD in the late half of the 21st century under the RCP 8.5 scenario by the regression model (same as Fig. 9), and contributions from each component, (e)-(h) precipitation, (j)-(i) bareness, and (m)-(p) surface wind speed. Dotted areas are regions with sign agreement among the models above 62.5%. To highlight DOD variations near the source regions, a mask of $LAI \leq 0.5$ (from present-day climatology) is applied.